HHS Public Access

Author manuscript

Sci Transl Med. Author manuscript; available in PMC 2024 April 15.

Published in final edited form as:

Sci Transl Med. 2018 September 19; 10(459): . doi:10.1126/scitranslmed.aao5620.

Axonal organization defects in the hippocampus of adult conditional BACE1 knockout mice

Ming-Hsuan Ou-Yang[1], **Jonathan E. Kurz**[2], **Toshihiro Nomura**[3,4], **Jelena Popovic**[1], **Tharinda W. Rajapaksha**[1], **Hongxin Dong**[5], **Anis Contractor**[3,4], **Dane M. Chetkovich**[3,6,#], **Warren G. Tourtellotte**[6,7,§], **Robert Vassar**[1,*]

[1]Department of Cell and Molecular Biology, Feinberg School of Medicine, Northwestern University, Chicago, IL 60611, USA

[2]Department of Pediatrics, Feinberg School of Medicine, Northwestern University, IL 60611, USA

[3]Department of Physiology, Feinberg School of Medicine, Northwestern University, IL 60611, USA

[4]Department of Neurobiology, Weinberg College of Arts and Sciences, Northwestern University, Evanston, IL 60208, USA

[5]Department of Psychiatry and Behavioral Sciences, Feinberg School of Medicine, Northwestern University, IL 60611, USA

[6]Department of Neurology and Clinical Neurosciences, Feinberg School of Medicine, Northwestern University, IL 60611, USA

[7]Department of Pathology, Division of Neuropathology, Feinberg School of Medicine, Northwestern University, Chicago, IL 60611, USA

Abstract

BACE1 is the β-secretase enzyme that initiates production of the toxic Aβ peptide that accumulates in the brains of patients with Alzheimer's disease (AD). As such, BACE1 is a prime therapeutic target and several BACE1 inhibitor drugs are currently being tested in clinical trials for AD. However, the safety of BACE1 inhibition is unclear. Germline BACE1 knockout mice have multiple neurological phenotypes, although these could arise from BACE1 deficiency during development. To address this question, we report that tamoxifen-inducible conditional BACE1 knockout mice in which the *Bace1* gene was ablated in the adult largely lacked the phenotypes observed in germline BACE1 knockout mice. However, one BACE1-null phenotype was induced after *Bace1* gene deletion in the adult mouse brain. This phenotype showed reduced length and disorganization of the hippocampal mossy fiber infrapyramidal bundle, the axonal pathway of

*Corresponding author. Robert Vassar. r-vassar@northwestern.edu.

#Current address: Department of Neurology, Vanderbilt University Medical Center, Nashville, TN 37232, USA

§Current address: Departments of Pathology and Laboratory Medicine, Departments of Neurology, Neurological Surgery, and Board of Governors Regenerative Medicine Institute, Cedar-Sinai Medical Center, Los Angeles, CA 90048, USA

Author contributions: M. O., W.G.T. and R.V. conceived the project and designed the study. M.O. performed and analyzed behavioral, biochemical and histology experiments. J. K. and D. M. C. contributed to EEG experiments. T. N. and A. C. contributed to the electrophysiological experiments. J. P. assisted M.O. in conducting experiments. H.D. contributed to behavioral study. T. W. R. screened and established BACE1$^{fl/fl}$ mouse lines. M.O. and R. V. wrote the manuscript with comments from all authors.

Competing interests: The authors declare no competing interests.

Data and materials availability: All data associated with this study are in the paper or supplementary materials.

dentate gyrus granule cells that is maintained by neurogenesis in the mouse brain. This defect in axonal organization correlated with reduced BACE1-mediated cleavage of the neural cell adhesion protein CHL1, which has previously been associated with axon guidance. Although our results indicate that BACE1 inhibition in the adult mouse brain may avoid phenotypes associated with BACE1 deficiency during embryonic and postnatal development, they also suggest that BACE1 inhibitor drugs developed for treating AD may disrupt the organization of an axonal pathway in the hippocampus, an important structure for learning and memory.

Introduction

Cerebral accumulation of amyloid-β peptide (Aβ) is a defining pathological hallmark of Alzheimer's disease (AD) and a large body of evidence indicates that Aβ is involved in the pathogenesis of this devastating neurodegenerative disorder (1, 2). Aβ is derived from the proteolytic processing of a large type-I membrane protein, the amyloid precursor protein (APP) (3). Two proteases, the β-secretase and the γ-secretase, sequentially cut APP to generate Aβ (4). β-site APP cleaving enzyme 1 (BACE1) has been identified as the β-secretase protease that cleaves APP to initiate the production of neurotoxic Aβ (5–9). Inhibition of BACE1 and thus Aβ production has therefore emerged as a leading therapeutic intervention for AD. However, the safety of BACE1 inhibition has been questioned, because BACE1 has a wide array of substrates, and proper cleavage of these substrates may be necessary for normal physiology (10–12). Germline BACE1 knockout ($BACE1^{-/-}$) mice lack Aβ production (13–15), thereby providing *in vivo* validation for BACE1 inhibition as a therapeutic approach for AD. However, $BACE1^{-/-}$ mice have been reported to exhibit smaller postnatal size and compromised survival (16), hypomyelination (17, 18), spontaneous seizures and abnormal electroencephalograms (EEGs) (19, 20), memory deficits (21, 22), and axon guidance defects (23–26) among other phenotypes (27). Previously, we reported that $BACE1^{-/-}$ mice phenocopy the axon guidance defects of CHL1 knockout mice in the hippocampus and olfactory bulb (24), indicating that BACE1 cleavage of CHL1 has a role in axonal targeting in these brain regions. However, since $BACE1^{-/-}$ mice are devoid of BACE1 from the moment of conception, the extent to which axon guidance defects and other BACE1-null phenotypes are related to BACE1 deficiency during development versus absence of BACE1 in the adult is unknown. This question has critical implications for the treatment of elderly AD patients with BACE1 inhibitor drugs, several of which are being tested in clinical trials (11, 28).

Here, we show that neurological phenotypes associated with germline BACE1 deficiency are reduced to a great extent, or eliminated altogether, in mice in which the BACE1 gene was inducibly deleted in the whole body of the adult. Importantly, however, adult conditional BACE1 knockout mice exhibited no reduction in the severity of axonal disorganization in the mossy fiber pathway of the hippocampus. The mossy fiber phenotype correlated with deficient BACE1 cleavage of CHL1, which regulates growth cone collapse via semaphorin 3A (26), an axon guidance molecule.

Results

Generation and characterization of conditional BACE1 knockout mice

To investigate the consequences of BACE1 inactivation in adults, conditional BACE1 knockout mice were generated in which exon 2 of the murine BACE1 gene was flanked with loxP sites (BACE1$^{fl/fl}$) by gene targeting (Fig. S1). BACE1$^{fl/fl}$ mice were then crossed to either CamKIIα-iCre mice (29) that express Cre recombinase in early postnatal forebrain excitatory neurons (BACE1$^{fl/fl}$;CamKIIα-iCre; Fig. S2A) or R26CreER^{T2} mice (30) that express from the ROSA26 locus a Cre recombinase fused to the estrogen receptor, thus enabling ubiquitous temporally controlled BACE1 gene deletion with administration of tamoxifen (BACE1$^{fl/fl}$;R26CreER^{T2}-TAM; Fig. S2B). We anticipated that BACE1$^{fl/fl}$;CamKIIα-iCre mice should begin excising exon 2 of the BACE1 gene in excitatory forebrain neurons around postnatal day 3 (29), with BACE1 exon 2 excision occurring in all cells of the body at any time upon treatment of BACE1$^{fl/fl}$;R26CreER^{T2} mice with tamoxifen (30).

We first verified BACE1 ablation in our conditional knockout mice by immunoblotting and immunohistochemistry (Fig. 1; Fig. S3). In BACE1$^{fl/fl}$;CamKIIα-iCre mice, cortical BACE1 in mouse brain dropped below detection beyond postnatal day 4 and was accompanied by accumulation of full-length BACE1 substrates and reduced cleaved fragments (Fig. 1A). In BACE1$^{fl/fl}$;R26CreER^{T2} mice treated with tamoxifen at 3 months and analyzed at 12 months of age, we observed ~90–95% reduction of BACE1 in cortex and hippocampus of mouse brain (Fig. 1D-G). Immunostaining for BACE1 in the mouse brain showed distinct patterns between the postnatal forebrain excitatory neuron knockout in BACE1$^{fl/fl}$;CamKIIα-iCre and the adult whole body knockout in BACE1$^{fl/fl}$;R26CreER^{T2} mice treated with tamoxifen (Fig. S3). BACE1 was virtually undetectable in forebrain regions, whereas cerebellum and brainstem exhibited BACE1 immunostaining in BACE1$^{fl/fl}$;CamKIIα-iCre mouse brain (Fig. S3A). In contrast, BACE1$^{fl/fl}$;R26CreER^{T2}mice treated with tamoxifen exhibited little BACE1 immunostaining in cerebellum and brainstem, whereas residual BACE1 immunostaining was observed in subcortical regions and olfactory bulb. We attribute the small amount of BACE1 immunostaining in BACE1$^{fl/fl}$;R26CreER^{T2}-tamoxifen treated mice to slight variability in penetration of tamoxifen into different brain regions. Importantly, despite the low residual BACE1 immunostaining detected (in hippocampus, for example; Fig. S3B, C), our immunoblot analysis confirmed that BACE1$^{fl/fl}$;R26CreER^{T2}-tamoxifen treated mice exhibited robust ~90–95% BACE1 reduction in cortex and hippocampus (Fig. 1D-G). To ensure that R26CreER^{T2} was tightly controlled by tamoxifen treatment, we examined BACE1 by immunoblotting in untreated BACE1$^{fl/fl}$;R26CreER^{T2} mice compared to wild-type mice (Fig. S4A). Quantification of BACE1 immunosignal showed no change in BACE1 (Fig. S4B), demonstrating that R26CreER^{T2} was tightly regulated and was completely inactive in the absence of tamoxifen.

After establishing that we were able to induce efficient postnatal forebrain or adult whole-body BACE1 reduction in our conditional knockout mice, we determined the effects of conditional BACE1 gene deletion on the processing of several major BACE1 substrates: APP (5–9), close homolog of L1 (CHL1) (31, 32), neuregulin 1 (NRG1) (17, 18),

and seizure 6 (Sez6) (32). As expected for BACE1 substrates, in BACE1$^{fl/fl}$;CamKIIα-iCre whole brain and cortex we observed increased full-length APP, CHL1, Sez6, and α-secretase-cleaved APP C-terminal fragment (α-CTF), and decreased BACE1-cleaved fragments of CHL1, NRG1, Sez6, and APP β-CTF (Fig. 1A-C). The effect of BACE1 conditional knockout on BACE1 substrates in the cortex and hippocampus of BACE1$^{fl/fl}$;R26CreER^{T2}-tamoxifen-treated mice followed similar but less pronounced and more variable changes, displaying increases in full length APP, α-CTF, full length CHL1, and full length Sez6 and decreases in BACE1-cleaved fragments of CHL1, APP, NRG1, and Sez6 (Fig. 1D-H). The greater inhibition of substrate processing observed in BACE1$^{fl/fl}$;CamKIIα-iCre mice compared to BACE1$^{fl/fl}$;R26CreER^{T2}-tamoxifen-treated mice was consistent with the greater reduction of BACE1 in postnatal forebrain relative to adult whole body BACE1 conditional knockout. Overall, we did not observe gender differences in the effects of conditional BACE1 knockout on cleavage of BACE1 substrates.

Postnatal lethality and underweight phenotypes are reduced or absent when *Bace1* is conditionally deleted

Next, we determined the phenotypic effects of BACE1 reduction in both of our BACE1 conditional knockout mouse lines. BACE1$^{-/-}$ mice have a high mortality rate in early postnatal development and are also smaller than their aged-matched heterozygous or wild-type littermates (16). When BACE1 was ablated in forebrain excitatory neurons at the postnatal stage, lethality and underweight phenotypes were greatly reduced in BACE1$^{fl/fl}$;CamKIIα-iCre mice (Fig. S5A-C). In a BACE1$^{fl/fl}$xBACE1$^{fl/fl}$;CamKIIα-iCre cross, BACE1$^{fl/fl}$;CamKIIα-iCre offspring survived nearly as well as BACE1$^{fl/fl}$ control offspring at the expected 50% rate (Fig. S5A, B) and were born underweight but reached almost normal weight by 3 months of age (Fig. S5C). In contrast, in a BACE1$^{+/-}$xBACE1$^{-/-}$ cross, BACE1$^{-/-}$ offspring exhibited marked mortality and those that survived remained severely underweight. When we conditionally ablated BACE1 in the whole body of the adult, we did not observe any lethality related to BACE1 reduction in BACE1$^{fl/fl}$;R26CreER^{T2}-tamoxifen treated mice (n=78) between the ages of 3 to 9 months. Unexpectedly, BACE1$^{fl/fl}$;R26CreER^{T2}-tamoxifen treated mice exhibited a weight gain following adult whole body BACE1 conditional knockout (Fig. S5D). Whereas BACE1$^{-/-}$ mice were reported leaner with enhanced insulin sensitivity (33), glucose and insulin metabolism of BACE1$^{fl/fl}$;R26CreER^{T2}-tamoxifen treated mice were similar to control BACE1$^{fl/fl}$-tamoxifen treated mice 7 months following BACE1 gene deletion (Fig. S5E-H). We also monitored energy metabolism activity in automated phenotyping chambers, but found no differences in feeding, drinking, locomotor activity, energy expenditure and fuel utilization between BACE1$^{fl/fl}$;R26CreER^{T2}-tamoxifen treated and control BACE1$^{fl/fl}$-tamoxifen treated mice (Fig. S6). Finally, necropsy of BACE1$^{fl/fl}$;R26CreER^{T2}-tamoxifen treated mice demonstrated that major tissues were histologically normal (Fig. S9). Although the basis of the weight gain observed in BACE1$^{fl/fl}$;R26CreER^{T2}-tamoxifen treated mice is currently unknown, together our results suggest that the reduced survival and weight of BACE1$^{-/-}$ mice may be caused mainly by BACE1 deficiency during early development.

Conditional BACE1 knockout mice are cognitively normal, but exhibit signs of hyperactivity

We next evaluated learning and memory function in our conditional BACE1 knockout mice, as BACE1$^{-/-}$ mice were previously reported to have memory deficits as early as 3 months of age (21, 22). BACE1$^{fl/fl}$;CamKIIα-iCre mice had normal memory at 6 months of age, despite showing delayed learning in the Morris water maze on day 2 of training (Fig. S7). At 9 months of age, delayed learning of BACE1$^{fl/fl}$;CamKIIα-iCre mice in the Morris water maze became more pronounced (Fig. 2A), yet memory impairment was not observed in the Morris water maze probe trial (Fig. 2B), spontaneous alternation in the Y-maze (Fig. 2E), and contextual (Fig. 2G) and cued (Fig. 2I) fear conditioning. As with germline BACE1 knockout mice (21), hippocampal CA1 longterm potentiation (LTP) in 1-year old BACE1$^{fl/fl}$;CamKIIα-iCre mice showed no deficit (Fig. 2K, L). This was consistent with the absence of memory impairment in postnatal forebrain neuron BACE1 conditional knockout mice. We then tested learning and memory function in BACE1$^{fl/fl}$;R26CreER^{T2} mice treated with tamoxifen at 3 months of age and assessed at 9 months of age (6 months following *Bace1* gene deletion). We observed that they performed comparably to BACE1$^{fl/fl}$-tamoxifen treated mice in all tests, but without the delayed learning found in BACE1$^{fl/fl}$;CamKIIα-iCre mice in the Morris water maze (Fig. 2C, D, F, H, J). Hippocampal CA1 LTP of the BACE1$^{fl/fl}$;R26CreER^{T2}-tamoxifen treated mice was also normal (Fig. 2M, N). We assessed locomotor activity of the mice in the open field test and while there were no differences in basal motor activity for either conditional knockout line (Fig. S8A, B), we observed longer travel distances in the open field (Fig. S8C) and greater arm entries in the Y-maze for BACE1$^{fl/fl}$;CamKIIα-iCre mice (Fig. S8E), suggesting novelty-induced hyperactivity as reported previously in BACE1$^{-/-}$ mice (21, 34). BACE1$^{fl/fl}$;R26CreER^{T2}-tamoxifen treated mice also exhibited greater arm entries in the Y-maze (Fig. S8F), but did not show longer travel distance in the open field test (Fig. S8D). Together, these results suggest that although conditional *Bace1* gene inactivation may be associated with hyperactivity, it does not cause memory deficits if it occurs in postnatal development or in the adult.

Adult whole-body conditional BACE1 knockout mice lack epileptiform abnormalities and hypomyelination

Spontaneous seizure and abnormal EEGs are other adverse phenotypes that have been reported in BACE1$^{-/-}$ mice (19, 20). To assess seizure activity in our conditional BACE1 knockout mice, we counted the number of spontaneous seizures and subjected mice to EEG recording and video monitoring. We observed a low penetrance of spontaneous seizures in our BACE1$^{fl/fl}$;CamKIIα-iCre colony, in which we counted 18 seizures in 15 mice (3 mice had 2 seizures each) out of a total of 83 mice over 2 months of random monitoring. In contrast, over the same period no spontaneous seizures were observed in 86 BACE1$^{fl/fl}$;R26CreER^{T2}-tamoxifen treated and 62 BACE1$^{fl/fl}$-tamoxifen treated mice. We selected one cohort in our BACE1$^{fl/fl}$;CamKIIα-iCre colony for EEG assessment, with 8 mice exhibiting spontaneous seizures from a group of 25 at 1 year of age. Of the 8 mice that exhibited seizures, seven survived surgery and three had spontaneous seizures captured within the 5-day recording period. An EEG trace of a representative generalized tonic-clonic seizure is presented in Fig 3A (lower trace) compared to a littermate BACE1$^{fl/fl}$ control mouse with a normal EEG (upper trace). Both single and

poly spike-wave discharges were observed in EEGs of BACE1$^{fl/fl}$;CamKIIα-iCre mice (Fig. 3B). Overall, BACE1$^{fl/fl}$;CamKIIα-iCre mice presented significantly (p=0.0003) more epileptiform events (3.5 spike-wave discharges/hr) than their BACE1$^{fl/fl}$ littermate controls (Fig. 3C), although they did not exhibit as many spike-wave discharges /hr as BACE1$^{-/-}$ mice (>40 spike-wave discharges /hr) (19, 20) indicating less severe seizure activity in postnatal forebrain neuron conditional BACE1 knockout mice compared to germline BACE1 knockout animals. Notably, we did not observe any spontaneous seizure activity in BACE1$^{fl/fl}$;R26CreER^{T2}-tamoxifen treated mice. EEG recordings from BACE1$^{fl/fl}$;R26CreER^{T2} mice treated with tamoxifen at 3 months and analyzed at 1 year of age (9 months following *Bace1* gene deletion) showed no seizures or abnormal EEG activity compared to control BACE1$^{fl/fl}$-tamoxifen treated mice (Fig. 3B, C). These results suggest that spontaneous seizures and abnormal EEGs derive from BACE1 deficiency during early postnatal development of excitatory forebrain neurons, but that BACE1 conditional knockout in adult neurons may not lead to epileptiform activity.

BACE1$^{-/-}$ mice were reported to have hypomyelination from insufficient BACE1 cleavage of NRG1 and impaired downstream signaling (17, 18). To determine whether our BACE1 conditional knockout mice also exhibited hypomyelination, we performed immunoblot analysis of cortex and sciatic nerve homogenates for myelin basic protein (MBP) and myelin proteolipid protein (PLP), and stained brain sections with Luxol fast blue for white matter. Immunoblot analysis revealed reduced MBP and PLP in the brains of postnatal day (P) 21 and P30 BACE1$^{fl/fl}$;CamKIIα-iCre mice (Fig. 1A). In contrast, we found no difference in central nervous system (CNS) myelination in BACE1$^{fl/fl}$;R26CreER^{T2} mice treated with tamoxifen at 3 months and analyzed at 12 months (9 months following *Bace1* gene deletion) either by cortical or hippocampal MBP immunoblotting (Fig. 1D, E) or Luxol fast blue staining of brain sections (Fig. 4C). Similarly, while immunoblot analysis of sciatic nerve homogenates from BACE1$^{fl/fl}$;R26CreER^{T2}-tamoxifen treated mice showed undetectable BACE1, we found no change in MBP compared to BACE1$^{fl/fl}$-tamoxifen treated control or BACE1$^{+/+}$ mice, even though BACE1$^{-/-}$ sciatic nerve homogenates displayed a significant reduction of MBP (p=0.006) (Fig. 4A, B). We further measured myelin thickness and calculated g-ratios in semi-thin sciatic nerve sections of BACE1$^{fl/fl}$;R26CreER^{T2}- tamoxifen treated mice along with BACE1$^{fl/fl}$- tamoxifen treated, BACE$^{-/-}$ and BACE1$^{+/+}$ control animals. Sciatic nerve of BACE1$^{-/-}$ mice, as previously reported (17, 18), exhibited reduced myelin sheath thickness around axons (Fig. 4D) and significantly (p<0.0001) increased g-ratio (Fig. 4E) indicating hypomyelination. In contrast, BACE1$^{fl/fl}$;R26CreER^{T2}-tamoxifen treated mice displayed normal myelin sheath thickness and a g-ratio similar to BACE1$^{fl/fl}$-tamoxifen treated mice and BACE1$^{+/+}$ mice (Fig. 4D, E). Thus, although postnatal forebrain neuron *Bace1* gene deletion is associated with hypomyelination, BACE1 conditional knockout in the adult whole body did not seem to affect central or peripheral myelination once development was completed.

Adult conditional BACE1 knockout mice exhibit axonal organization defects in the hippocampus

Previously, we determined that BACE1$^{-/-}$ mice exhibited axonal organization defects that correlated with deficient processing of the neural cell adhesion molecule CHL1 (24). CHL1

is a substrate that appears to be preferred by BACE1 in neurons (31, 32). Consistent with these observations, BACE1-cleaved CHL1 β-NTF and full length CHL1 were decreased and increased, respectively, in the brains of BACE1$^{fl/fl}$;CamKIIα-iCre mice (Fig. 1A) and BACE1$^{fl/fl}$;R26CreER^{T2}-tamoxifen treated mice (Fig. 1D-G). Interestingly, differences in CHL1 β-NTF and full length CHL1 between BACE1$^{fl/fl}$;R26CreER^{T2}-tamoxifen treated mice and BACE1$^{fl/fl}$-tamoxifen treated control mice were substantial, suggesting that induced deletion of the *Bace1* gene in the adult may affect the function of CHL1 even after development is completed.

One of the CHL1-correlated axonal abnormalities that we had observed in the brains of germline BACE1 knockout mice was a disorganized and shortened length of the infrapyramidal bundle of the hippocampal mossy fiber pathway and premature crossing of the CA3 pyramidal cell layer (24). To determine whether deficient BACE1 cleavage of CHL1 correlated with axonal defects in adult mice, we measured the length and assessed the organization of the infrapyramidal bundle of BACE1$^{fl/fl}$;R26CreER^{T2}-tamoxifen treated mice in coronal brain sections immunostained for BACE1 and the mossy fiber marker synaptoporin (Fig. 5A S15). Similar to BACE1$^{-/-}$ mice, infrapyramidal bundle length was shorter in BACE1$^{fl/fl}$; CamKIIα-iCre mice compared to BACE1$^{fl/fl}$ mice at 9 month of age (Fig. 5A, C). Importantly, BACE1$^{fl/fl}$;R26CreER^{T2} mice treated with tamoxifen at 3 months and analyzed at 1 year of age (9 months following *Bace1* gene deletion) had significantly shorter infrapyramidal bundle length ($p=1.4\times10^{-5}$) compared to BACE1$^{fl/fl}$-tamoxifen treated negative control mice (Fig. 5A, C). The amount that the infrapyramidal bundle was shortened in the adult conditional knockout mice (~30%) was similar to that observed in BACE1$^{-/-}$ mice (Fig. 5C) reported in our previous study (24). Also similar to BACE1$^{-/-}$ mice, we observed that the organization of the infrapyramidal bundle of BACE1$^{fl/fl}$;R26CreER^{T2}-tamoxifen treated mice was severely disrupted compared to that of BACE1$^{fl/fl}$-tamoxifen treated mice, exhibiting premature crossing of mossy fibers through the CA3 pyramidal cell layer (Fig. 5B); this is a phenocopy of CHL1 knockout mice (35, 36). Immunostaining with an anti-CHL1 antibody revealed co-localization of CHL1 with presynaptic terminal and mossy fiber bouton markers synaptophysin and calbindin, respectively (Fig. 5B, low power image in Fig. S14), indicating neuronal, and specifically presynaptic, CHL1 localization. As we have previously reported, CHL1 also co-localized with BACE1 in mossy fiber terminals in the hippocampus (24).

Next, we performed immunoblot analysis for CHL1 to determine the extent of BACE1 cleavage of CHL1 in the hippocampus of the adult conditional BACE1 knockout and control mice. As expected, we found that CHL1 β-NTF and full length CHL1 were decreased and increased in soluble and membrane fractions of hippocampal homogenates, respectively, in BACE1$^{fl/fl}$;R26CreER^{T2}-tamoxifen treated mice compared to BACE1$^{fl/fl}$-tamoxifen treated mice (Fig. 5D, E). Linear regression analysis showed that infrapyramidal bundle length positively and negatively correlated with soluble CHL1 and the ratio of full length CHL1 to β-NTF, respectively (Fig. 5F, G). Taken together, these results demonstrate that processing of CHL1 by BACE1 is active in the adult brain and is correlated with the maintenance of the normal structure of a major axonal pathway in the hippocampus that is involved in learning and memory.

We and others have previously reported that BACE1 deficiency results in disorganization and mis-targeting of olfactory sensory neuron axons in the glomeruli of the olfactory bulb (23–25), which is also a phenocopy of CHL1$^{-/-}$ mice (35, 36). Therefore, we determined whether adult conditional BACE1 knockout disrupted olfactory sensory neuron axonal organization in the olfactory bulb. First, we performed immunoblot analysis of olfactory bulb homogenates from the 1 year-old BACE1$^{fl/fl}$;R26CreER^{T2} mice and BACE1$^{fl/fl}$ mice treated with tamoxifen at 3 months and observed only ~25–30% reduction of BACE1 in the olfactory bulbs of adult conditional BACE1 knockout mice (Fig. S10A, B). We hypothesized that this modest BACE1 reduction was insufficient to result in disorganization of olfactory sensory neuron axons in the olfactory bulb. To test this, we immunostained olfactory bulb sections of the BACE1$^{fl/fl}$;R26CreER^{T2}-tamoxifen treated mice and BACE1$^{fl/fl}$-tamoxifen treated mice with an antibody against olfactory marker protein, which labels axons and termini of olfactory sensory neurons. Indeed, we found no evidence of abnormal axonal organization in the olfactory nerve layer or glomeruli of BACE1$^{fl/fl}$;R26CreER^{T2} mice treated with tamoxifen compared to BACE1$^{fl/fl}$ mice treated with tamoxifen (Fig. S10C, D). An analysis of the circularity of glomeruli of adult conditional BACE1 knockout mice also revealed no differences compared to controls (Fig. S10E).

Axonal organization defects in adult conditional BACE1 knockout mice are not associated with abnormal adult neurogenesis or apoptosis

Because of the similar infrapyramidal bundle phenotypes of CHL1$^{-/-}$, BACE1$^{-/-}$, and adult conditional BACE1 knockout mice, and since processing of CHL1 by BACE1 regulates growth cone collapse via a pathway involving the axon guidance molecule semaphorin 3A (26), we hypothesized that deficient BACE1 cleavage of CHL1 resulted in an axon guidance defect that caused the shortened and disorganized infrapyramidal bundle of the adult conditional BACE1 knockout mice. However, other mechanisms besides axon guidance could contribute to the infrapyramidal bundle phenotype associated with BACE1 deficiency. For example, CHL1 has been reported to affect multiple physiological processes, including cell proliferation (37), apoptosis (38), neurite outgrowth (39, 40), neuronal differentiation (37, 41), serotonin receptor signaling (42), and area-specific neuronal positioning and dendrite orientation (43, 44), any of which could potentially influence the organization and length of the infrapyramidal bundle. Additionally, germline BACE1 knockout mice exhibit increased neurodegeneration with age (19) and an altered balance between hippocampal astrogenesis and neurogenesis (45) that might also contribute to the BACE1-null infrapyramidal bundle phenotype.

To begin to approach these questions, we investigated neural progenitor cell proliferation, adult neurogenesis, and apoptosis, which are major processes in the dentate gyrus that could affect the infrapyramidal bundle of adult conditional BACE1 knockout mice. BACE1$^{fl/fl}$;R26CreERT^{2} and BACE1$^{fl/fl}$ mice treated with tamoxifen at 6–9 months were aged to 2 years (15–18 months following *Bace1* gene deletion), injected with BrdU, and brains were harvested 24 hours and 1 month after the last BrdU injection. BACE1 immunoblots of hemibrain homogenates from each mouse revealed that BACE1 was reduced by ~90% in BACE1$^{fl/fl}$;R26CreERT^{2}-tamoxifen treated mice (Fig. S11A), indicating efficient induction of *Bace1* gene deletion in the adult brain. We also verified that the BrdU labeled

BACE1$^{fl/fl}$;R26CreERT^{2}-tamoxifen treated mice exhibited a shortened and disorganized infrapyramidal bundle phenotype similar to that present in other adult conditional BACE1 knockout mice (S11B). Coronal sections of the other hemibrain from each mouse were prepared and co-labeled with either anti-BrdU antibody and DAPI (24-hour post-BrdU) or anti-BrdU and anti-NeuN antibodies (1-month post-BrdU) (Fig. S12A).

First, we found no differences in either the volume of the dentate gyrus or the number of BrdU-positive cells/mm^{3} in 24-hour post-BrdU brain sections (Fig. S12B-C), indicating that overall neural progenitor cell proliferation in the subgranular zone and the size of the dentate gyrus were not affected by adult conditional BACE1 knockout. We noted that the rates of neurogenesis in these aged mice were low compared to rates for young mice, but were within the range expected for 2-year old mice (46). Next, we observed that the percentage of BrdU+NeuN double-positive neurons in the granule cell layer of the dentate gyrus in 1-month post-BrdU brain sections was unchanged in BACE1$^{fl/fl}$;R26CreERT^{2}-tamoxifen treated mice (Fig. S12D), suggesting that the differentiation of newly born neurons occurred normally after *Bace1* gene ablation in the adult. Since topographic differences in adult neurogenesis are present in the hippocampus (47), we analyzed the regional distributions of dividing cells and newly born neurons in the suprapyramidal blade, infrapyramidal blade, and crest of the dentate gyrus (Fig. S12F, G). We determined that adult conditional inactivation of BACE1 was not associated with regional differences in either the total estimated number of BrdU positive cells per dentate gyrus in 24-hour post-BrdU sections (Fig. S12F) or the percentage of BrdU+NeuN double-positive neurons in 1-month post-BrdU sections (Fig. S12G).

Finally, to assess a potential role for apoptosis in the BACE1-deficient infrapyramidal bundle phenotype, we performed TUNEL assays on brain sections from the 24-hour BrdU-labeled mice. Notably, no TUNEL-positive granule cells were observed in sections of the dentate gyrus of BrdU-labeled BACE1$^{fl/fl}$;R26CreERT^{2}-tamoxifen treated and BACE1$^{fl/fl}$-tamoxifen treated mice, despite the presence of TUNEL-positive cells in other areas of the hippocampus (Fig. S13).

Discussion

Here, we generated conditional *Bace1* knockout mice to determine whether BACE1 is required in the adult for normal structure and function. Several of the neurological phenotypes of germline BACE1 knockout mice were absent following adult conditional BACE1 gene deletion. Importantly, however, when we allowed the brain to develop with BACE1 and then ablated BACE1 after adulthood was achieved, we observed that the infrapyramidal bundle of the hippocampal mossy fiber pathway was disorganized and exhibited a shortened length, possibly as the result of a defect in axon guidance. BACE1 is highly concentrated in hippocampal mossy fibers (48, 49), perhaps for the continuing requirement of adult axon guidance (50, 51). Indeed, CHL1 is a BACE1 substrate (31, 32), and we have shown that BACE1$^{-/-}$ mice phenocopy the axon organization defects of CHL1 knockout mice (24). Moreover, the cleavage of CHL1 by BACE1 regulates the balance between growth cone extension and collapse via the axon guidance molecule semaphorin 3A (26), a process critical for correct axonal targeting. Future studies are necessary to

determine whether axonal disorganization exists beyond the hippocampus in other regions of the brain of adult conditional BACE1 knockout mice. Additionally, treatment of wild-type mice with a BACE1 inhibitor should be performed to determine whether infrapyramidal bundle organizational defects occur following pharmacological BACE1 inhibition.

Neurogenesis of dentate gyrus granule cells is known to continue in the subgranular zone of the hippocampus during adulthood (52). Consequently, mossy fiber axons of granule cells born in the adult require axon guidance to find their correct target neurons in the hippocampal CA3 region. Mossy fiber axons of newly-born granule cells in the infrapyramidal blade of the dentate gyrus grow for a distance along the ventral side of the CA3 pyramidal cell layer, thus forming the infrapyramidal bundle. The axons then invade the cell layer and cross to the dorsal side where they merge into the stratum lucidum and join other mossy fiber axons that come from the suprapyramidal blade of the dentate gyrus. The factors that determine the distance that mossy fibers grow before crossing the CA3 pyramidal cell layer, and therefore the length of the infrapyramidal bundle, are not yet fully elucidated, but correlate with CHL1 processing by BACE1 (24). Interestingly, the length of the infrapyramidal bundle varies between different inbred strains of mice, and longer infrapyramidal bundle lengths correlate with better spatial orientation learning in the radial maze (53). Given this finding, it was unexpected that we did not observe memory deficits in adult conditional BACE1 knockout mice in our study. In future studies, it will be important to test adult conditional BACE1 knockout mice in more sensitive and varied behavioral paradigms, including the radial maze and Barnes maze that avoid the stress of swimming, to detect potential deficits in spatial orientation and other types of learning or memory with age. Moreover, germline BACE1 knockout mice have been reported to exhibit impaired mossy fiber-CA3 LTP (54, 55). Therefore, it will be important to determine whether adult conditional BACE1 knockout mice have a mossy fiber-CA3 LTP abnormality and, if so, understand its relationship to the infrapyramidal bundle and behavioral phenotypes.

Although we favor the hypothesis that deficient BACE1 cleavage of CHL1 causes defective axon guidance resulting in the short and disorganized infrapyramidal bundle of adult conditional knockout mice, other mechanisms, either involving CHL1 or not, could be responsible. Our BrdU and TUNEL experiments indicated that alterations in adult neurogenesis including overall or regional neural progenitor cell proliferation, neuronal differentiation, and apoptosis in the dentate gyrus were unlikely to produce the phenotype. However, we could not exclude other potential causes, such as abnormal neurite outgrowth, serotonin receptor signaling, area-specific neuronal positioning and dendrite orientation, neurodegeneration, or defective activity dependent axonal refining, among others.

It is possible that a combination of mechanisms may influence the length and organization of the infrapyramidal bundle. For example, impaired axon guidance together with axonal degeneration as observed in germline BACE1 knockout mice (19) may affect the infrapyramidal bundle. A study reported that only ~10% of dentate gyrus neurons are newly generated by adult neurogenesis in mice, although the authors noted that this number is an underestimate (56). The same authors also observed that relatively few dentate gyrus neurons die, and that the total number of granule cells continues to increase in the adult dentate gyrus. These results suggest that defective axon guidance of newly generated mossy

fibers together with degeneration of axons formed during development may contribute to the shortened and disorganized infrapyramidal bundle of adult conditional BACE1 knockout mice. Since BACE1 cleavage of CHL1 regulates growth cone collapse (26), it is possible that both axon guidance and mossy fiber degeneration are affected by CHL1 processing in the adult dentate gyrus. It will be important to conduct additional studies to investigate the potential roles of these and other mechanisms in determining the characteristics of the infrapyramidal bundle.

Our conditional BACE1 knockout mice have been useful for deciphering the roles of BACE1 in neurons during development versus the adult. Postnatal excitatory forebrain neuron conditional BACE1 knockout mice were partially protected from reduced survival, growth retardation, seizures, EEG abnormalities, and hypomyelination, and fully protected from memory deficits, while adult whole-body conditional BACE1 knockout mice completely lacked these adverse phenotypes. Therefore, we conclude that many of the neurological phenotypes of the germline BACE1 knockout mice are the result of BACE1 deficiency during nervous system development and do not result from absence of BACE1 function in the adult. This conclusion is also supported by the observation that BACE1 and some of its substrates like NRG1, and BACE1 itself, are highly expressed in the developing organism, especially in the nervous system (17, 18) implying critical functions for BACE1-cleaved substrates during neuronal proliferation, determination, differentiation, or maturation. A recent study investigating a different line of conditional BACE1 knockout mice has reported that amyloid plaques are reversible in adult conditional BACE1 knockout mice crossed to the 5XFAD amyloid pathology model (57), although this study did not analyze the infrapyramidal bundle (58).

We note that our study has several limitations. First, it is possible that other phenotypes besides the disorganized infrapyramidal bundle may have been detected in adult conditional BACE1 knockout mice if more sensitive assays were used. Also, we did not assess germline BACE1 knockout phenotypes involving astrogenesis, muscle spindles, neurochemical deficits, schizophrenia endophenotypes, or spine density. Another limitation of our study was variable BACE1 knockout in different brain regions, such that BACE1 knockout was 90–95% in some regions like hippocampus and cortex, while other regions had comparatively poor BACE1 knockout, as in the olfactory bulb. As this was likely the result of variable tamoxifen penetration, Cre driver mice that are induced by other molecules such as doxycycline may provide more complete BACE1 knockout in certain brain regions. Lastly, it is unclear how well our adult conditional knockout mouse results translate to humans treated with BACE1 inhibitors. Given the structural and functional complexity of the human brain, it is conceivable that more severe neurological phenotypes may arise as a result of BACE1 inhibition in elderly humans compared to conditional BACE1 knockout mice.

In conclusion, our results with adult conditional BACE1 knockout mice demonstrate that BACE1 continues to function after development to maintain normal axonal organization in the adult brain, at least in the mossy fiber pathway of the hippocampus. Regarding BACE1 inhibitors for Alzheimer’s disease, while these drugs have advanced into clinical trials, safety data from human and animal studies are just becoming available (59, 60).

By comparing previously known phenotypes in BACE1$^{-/-}$ mice to our BACE1 conditional knockout mice, our study provides valuable preclinical safety and tolerability information of relevance to the current BACE1 inhibitor trials and has also shown that several of the neurological phenotypes of the germline BACE1 knockout mice are the result of BACE1 deficiency during development rather than in the adult. On the other hand, the current human clinical trials of BACE1 inhibitors include doses that lower CSF Aβ up to ~90% (59, 61, 62). This represents strong inhibition of BACE1 comparable to the BACE1 reduction in the cortex and hippocampus of our adult conditional BACE1 knockout mice. The human trials will treat subjects for 18–24 months, although some prevention trials will treat for 5 years. Because of the short lifespan of the mouse, the adult conditional BACE1 knockout mice analyzed after 6 to 9 months of BACE1 deficiency represent a longer relative duration compared to the treatment times of the current clinical trials when normalized to human lifespan. Therefore, our experiments suggest that BACE1 inhibition may cause mechanism-based side effects that might not be revealed within the relatively short timeframe of the clinical trials. Interestingly, in contrast to the mouse, studies of hippocampal neurogenesis in humans indicate that most dentate gyrus neurons are exchanged in the adult (63). This suggests that the disorganization of dentate gyrus mossy fiber axons may be even more severe in humans exposed to chronic BACE1 inhibitor treatment than in adult mice induced by BACE1 inactivation. Because a patient will likely require chronic treatment with a BACE1 inhibitor drug for the remainder of life, our results strongly caution against aggressive BACE1 inhibition, or otherwise risk mechanism-based side effects in the adult hippocampus.

Materials and Methods

Study design

This study used a loxP-Cre recombinase genetic approach to conditionally delete the *Bace1* gene in mice to determine whether BACE1 is required in the adult animal to provide insights into mechanism-based side effects of BACE1 inhibitors in human clinical trials. Two conditional BACE1 knockout mouse strains were generated in this study: excitatory forebrain neuron BACE1$^{fl/fl}$;CamKIIα-iCre mice and adult tamoxifen inducible whole body BACE1$^{fl/fl}$; R26CreER^{T2}-TAM mice. To model patients under long-term BACE1 inhibition, all mice analyzed had at least 6 months of conditional BACE1 knockout. Previously published phenotypes associated with germline BACE1 knockout mice were analyzed in conditional BACE1 knockout mice including metabolism, seizures, axonal organization defects, behavioral abnormalities and learning/memory deficits.

For all experiments, sample sizes were determined based on our previous experience with germline BACE1 knockout mice and the literature, which proved to be sufficient to allow detection of statistically significant differences. Experimental methods chosen in the study were either previously published for analysis of germline BACE1 knockout mice or were widely accepted and well-established approaches. Outliers were excluded only in behavior analyses and only when the values were beyond two standard deviations of the mean. The number of biological replicates for each experiment is specified in the figure legends and elaborated in Materials and Methods. Mice were randomized in genotypes and sexes during

behavioral testing. For behavioral, EEG and LTP studies, experimenters were blinded during data acquisition and unblinded for data analysis.

Antibodies

Rabbit anti-actin (LICOR, 926–42210), rabbit anti-APP (Abcam, ab32136), mouse anti-BACE1 (3D5), rabbit anti-BACE1 (Abcam, ab108394), rat anti-BrdU (ThermoFisher, MA1–82088), rabbit anti-Calbindin (Cell Signaling, #2173), goat anti-CHL1 (R&D systems, AF2147), rat anti-Myelin Basic Protein (Abcam, ab7349), rabbit anti-Neuregulin type III (Millipore, AB5551), chicken anti-NeuN (Millipore, ABN91), goat anti-OMP (WAKO, 544–1001), mouse anti-βIII Tubulin (Tuj1) (gift from Dr. Lester Binder), rabbit anti-PLP (Abcam, ab28486), goat anti-synaptoporin (Santa Cruz, sc21212), mouse anti-synaptophysin (Millipore, MAB5258) and rat anti-Sez6 (gift from Dr. Stefan Lichtenthaler).

Animals

BACE1 ES cell clones in which BACE1 gene exon 2 (BACE1 floxed) was flanked by loxP sites were obtained from European Mouse Mutant Cell Repository (EuMMCR, ES cell line JM8A3.N1) and were grown under standard conditions by the Northwestern University Transgenic and Targeted Mutagenesis Laboratory. Southern blot verified clones were then microinjected to C57Bl/6 blastocysts. Chimeric mice were verified by tail DNA PCR using primers (5’ tgattcctttcattaagagg and 5’ ttaagcttatgtgtgccatc). BACE1 floxed mice ($BACE1^{fl/fl}$) were generated by crossing chimeric mice to CAG-FLPe mice to remove the FRT-flanked lacZ and neomycin cassette (Fig. S1). For the forebrain BACE1 conditional knockout study, $BACE1^{fl/fl}$ mice were crossed to heterozygous CamKIIα-iCre mice (29) to generate $BACE1^{fl/fl}$;CamKIIα-iCre heterozygous or $BACE1^{fl/fl}$;CamKIIα-iCre negative littermates, which served as controls for the study. For the adult whole-body inducible BACE1 knockout study, $BACE1^{fl/fl}$ mice were crossed to homozygous $R26CreER^{T2}$ mice (30) to generate $BACE1^{fl/fl}$;$R26CreER^{T2}$ homozygous mice. A separate cohort of $BACE1^{fl/fl}$ mice treated with tamoxifen was used as controls. Tamoxifen (MP Biomedicals, #156738) was dissolved in corn oil at 25 mg/ml. 3-month old $BACE1^{fl/fl}$;$R26CreER^{T2}$ mice were i.p. injected with tamoxifen at 100 mg/kg of weight daily for 5 days followed by 3 days of break (one cycle). Complete treatment consisted of 3 cycles of tamoxifen injection. Unless indicated, no significance was noted between the genders and the data presented was the mean of both male and female animals. All animal work was performed in accordance with Northwestern University IACUC approval.

Behavioral testing

Mice were allowed to acclimate to the testing environment at least 0.5 hour before tests. Mice were randomized by gender and genotypes to which the experimenter was blinded during the tests. Behavior tests were performed in the order described below.

Open field—The open field arena was a 55 cm wide x 55 cm long x 30 cm tall box. The mouse was placed in the middle of the box and allowed to explore the box for 15 minutes. Ambulation activity was tracked and quantified by LimeLight software (Actimetrics).

Y maze—The maze contained three identical arms of 42 cm long spaced 120 degrees apart radiating from a central triangular area. The mouse was placed at the base of the arm forming the stem of Y and allowed to freely traverse the maze for 8 minutes. Alternation score was calculated as the number of alternations divided by the number of possible alternations multiplied by 100, with a 50% score being random selection. Travel pathway was tracked by LimeLight software (Actimetrics).

Morris water maze—A platform of 8.5 cm diameter was submerged in opaque water in a quadrant of a pool with diameter of 1.8 m. Water remained at room temperature (22 °C±1) through all trials. Distinct visual cues were present in both hidden and probe trials. Hidden platform training was performed by giving 3 trials a day with 20–30 minutes between trials for five days. The probe trial for memory of the position of the hidden platform took place 24 hours after the last hidden platform training trial. Three visible platform trials were done right after probe trial on the same day to test for visual acuity. Tests were monitored and analyzed using ANY-maze software (San Diego Instruments, San Diego, CA).

Fear conditioning—A mouse was allowed to freely explore a testing chamber equipped with shock and tone (Harvard Instruments) for 2 minutes, then the mouse was subjected to a tone of 2.5 kHz for 30 seconds, during the last two seconds of which a 0.8 mV shock was applied. The mouse was then removed from the chamber 30 seconds after the shock and returned to the home cage. Contextual fear conditioning was tested 24 hours after training in which the mouse was re-exposed to the chamber for 2 minutes except no shock was applied. 48 hours after initial conditioning, cue fear conditioning was tested in which the mouse was exposed to a new environment with a novel odor for two minutes (pre-tone) then the tone but no shock was applied for another two minutes (tone). Freezing behavior was recorded and scored using ANY-maze software.

Tissue extraction and immunoblot analysis

Mice were deeply anesthetized by intraperitoneal injection of xylazine (15 mg/kg) and ketamine (100 mg/kg), perfused with ice-cold PBS with PMSF (20 μg/ml), leupeptin (0.5 μg/ml), sodium orthovanadate (20 μM) and DTT (0.1 mM), followed by decapitation and brain removal. The hemi-brain was dissected on ice into cortex, hippocampus, olfactory bulb, cerebellum and the rest of the brain, then snap-frozen in liquid nitrogen and stored at −80 °C. Tissues were homogenized in TBS followed by centrifugation at 20,800 × g for 20 minutes at 4 °C. The supernatant was removed as the soluble fraction and the pellet was extracted again in RIPA (50 mM Tris, 0.15 M NaCl, 1% IGEPAL, 1 mM EDTA, 1 mM EGTA, 0.1% SDS, 0.5% sodium deoxylate at pH 8), centrifuged and supernatant was removed as the membrane fraction. All buffers contained protease inhibitor cocktail III (Millipore, #535140) and Halt phosphatase inhibitor (Thermo Fisher, #78420). Alternatively, tissues were directly homogenized in RIPA buffer followed by centrifugation. The resulting supernatant was referred as total extraction. Protein concentration was determined using BCA assay (Thermo Fisher, #23225). Equal amount of protein was separated under reduced and denatured conditions, transferred onto PVDF membrane and developed using Pierce ECL (Thermo Fisher) on a ProteinSimple FCR imager. Chemiluminescent signals were quantified using AlphaView (ProteinSimple) software.

Immunohistochemistry

Hemi-brains were fixed in 10% formalin and preserved in 30% sucrose/PBS. Brains were sectioned at 30 μm on freezing-sliding microtome and stained using the free-floating method. Alexa Fluor secondary antibodies (Invitrogen) were used for immunofluorescence. For BrdU staining, sections were treated in 37 °C 2N HCl for 30 minutes and neutralized with 0.1 M borate buffer pH8.5 for 10 minutes at RT prior to blocking. Sections were mounted using Prolong Gold (Thermo Fisher, P36934) and imaged on Nikon A1 laser scanning confocal microscope (Northwestern University Center for Advanced microscopy). For DAB staining, biotinylated-secondary antibody was used followed by the ABC method (Vector lab).

Fast blue staining—De-paraffinized sections on glass slides were incubated in Luxol fast blue solution in a 60 °C oven overnight, de-stained with 95% ethanol and then distilled water, and differentiated in lithium carbonate solution and 70% ethanol. After rinsing with water, slides were dehydrated in graded ethanol series and mounted in permount.

Measurement of the infrapyramidal bundle

Detailed procedures for infrapyramidal bundle length analysis have been described previously (24). Briefly, 30μm coronal sections were labeled with antibodies against the mossy fiber marker synaptoporin (SPO) and BACE1. Confocal microscope images of the mossy fiber pathway were taken from sections near the rostral-caudal mid-line and the interblade line was made connecting the tips of the superior and inferior blades of the dentate gyrus. The length of SPB (beginning from the interblade junction to the point where SPB begins to taper outward), slu (from the point where SPB begins to taper outward to the distal end of the slu) and infrapyramidal bundle (from the end of pyramidal cell layer to the distal point of uninterrupted SPO staining beneath the pyramidal cell layer) were measured by free-hand tracing along the middle line of SPO staining in ImageJ. Three sections from each brain were measured and averaged.

Electrophysiology

Horizontal hippocampal slices were prepared as previously described (64). Briefly, animals were deeply anesthetized by intraperitoneal injection of xylazine (10 mg/kg) and ketamine (100 mg/kg), and cardiac perfusion was performed with an ice-cold sucrose artificial cerebrospinal fluid (ACSF) solution containing (in mM): 85 NaCl, 2.5 KCl, 1.25 NaH_2PO_4, 25 $NaHCO_3$, 25 glucose, 75 sucrose, 0.5 $CaCl_2$, and 4 $MgCl_2$ with (in μM) 0.01 DL-APV and 0.1 kynurenic acid equilibrated with 95% O_2 and 5% CO_2. The brain was quickly removed and horizontal sections (350 μm thick) were prepared in the same ice-cold sucrose ACSF using a Vibratome VTI 1200 (Leica Microsystems, Inc). Slices were transferred to a recovery chamber containing the same sucrose ACSF for ~15 min at 30 °C, and the solution was gradually exchanged for a recovery ACSF containing (in mM): 125 NaCl, 2.4 KCl, 1.2 Na_2PO_4, 25 $NaHCO_3$, 25 glucose, 1 $CaCl_2$, and 2 $MgCl_2$ with (in μM) 0.01 DL-APV and 0.1 kynurenic acid at room temperature. Individual slices were transferred to a recording chamber and visualized using Dodt contrast optics. During recordings, slices were continuously perfused with a normal ACSF containing (in mM): 125 NaCl, 2.4 KCl,

1.2 Na_2PO_4, 25 $NaHCO_3$, 25 glucose, 2 $CaCl_2$ and 1 $MgCl_2$. Recording electrodes were manufactured from borosilicate glass pipettes and had tip resistances of 3–5 MΩ when filled with ACSF. Extracellular field excitatory postsynaptic potentials (fEPSPs) were evoked using a monopolar electrode filled with ACSF placed in the stratum radiatum. fEPSPs were recorded within CA1 subregion of the hippocampus. After a stable fEPSP had been recorded for at least 10 min at a frequency of 0.05 Hz (using a response approximately 50% of the maximum), LTP was induced with three trains of 100 Hz for 1 s with an inter-train interval of 20 s. Data were collected and analyzed using pClamp 10 software (Molecular Devices, Sunnyvale, CA).

Animal Surgery, EEG recording

EEG was recorded using Pinnacle 2EEG/1EMG mouse EEG hardware with synchronized video, and was acquired using the Pinnacle Sirenia software suite (Pinnacle Inc, Lawrence, KS). Briefly, under isoflurane anesthesia, EEG/EMG headmounts were attached to the skull with 4 screws that serve as surface EEG electrodes and then were secured with dental acrylic. During the same surgery, 2 EMG electrodes were placed into the trapezius muscle. Animals were allowed to recover for 1 week prior to EEG recording. All animals were maintained on a 12h light/dark cycle and received 4 or 5 days of continuous EEG recording with synchronized video (with IR lighting for capture of video during dark phase). EEG data was visualized using the Sirenia software (Pinnacle Inc). To aid with seizure detection, additional signal processing was performed using MATLAB r2016a and the EEGLAB toolbox (Swartz Center for Computational Neuroscience, La Jolla, CA). The entire 5-day EEG recording was reviewed for electrographic seizures, with further review of the video for any periods suspicious for seizure. Total number of spike-wave discharges were determined over a 48 hour epoch. Single spikes were identified as sharp activity with an amplitude of at least twice baseline and associated with an aftercoming slow wave, while polyspikes were identified as multispike complexes with a spike/wave morphology and amplitude at least twice baseline. Comparison of the EEG signal to the EMG signal was used to exclude movement artifacts.

Sciatic nerve g-ratio analysis

Samples were fixed in 2% paraformaldehyde and 2.5% glutaraldehyde in 0.1 M sodium cacodylate buffer pH7.3 and post-fixed with unbuffered 2% osmium tetroxide, rinsed with distilled water, en-bloc stained with 3 % uranyl acetate, rinsed with distilled water, dehydrated in ascending grades of ethanol, transitioned with propylene oxide and embedded in resin mixture from the Embed 812 kit and cured in a 60 ˚C oven. Samples were sectioned on a Leica Ultracut UC6 ultramicrotome. 1μm thick sections were collected and stained with Toluidine Blue O. Images were taken under 100X and *Feret's* diameters were determined from hand-traced axons using the ImageJ built-in function. 100 axons were randomly sampled from each animal. G ratio was calculated by dividing inner axon diameter divided by outer diameter including the myelin sheath.

Glucose tolerance and insulin tolerance tests

Mice were fasted for 16 hours prior to the glucose tolerance test. Glucose was i.p. injected at 2 g/kg of body weight and blood glucose was determined using a standard glucose meter

(Precision Xtra glucose meter, Abbott). For the insulin tolerance test, mice were i.p. injected with Regular Human Insulin (Lily) at 0.75 U/kg of weight. Blood glucose was determined at 0, 15, 30, 60 and 120 minutes by Precision Xtra glucose meter (Abbott) and compatible glucose strips.

TSE LabMaster automated phenotyping

Mice were singly housed in their home cages in an enclosed environmental chamber of the TSE automated Phenotyping System (TSE Systems Inc. Chesterfield, MO) with controlled temperature under 12 hour light/ dark cycle at the Northwestern University Metabolic Phenotyping Core Facility. Data collection began after a three-day acclimation period. Food and fluid intake were continuously recorded via feeding/drinking sensors. Locomotor activities in 3 dimensions were monitored via infrared beam breaks through frames mounted on the perimeter of the metabolic cages, CO_2 production and O_2 consumption were used to assess energy expenditure and respiratory exchange ratio (RER). Data were averaged and plotted in 24hr duration since no differences between light and dark cycles was observed.

Necropsy

Necropsy was performed by Northwestern University Mouse Phenotyping and Histology Lab. Briefly, mice were anesthetized with lethal dose of ketamine/xylazine cocktail and perfused with equal volume of PBS and 4% PFA. Tissues were harvested, fixed in 10% formalin and processed for paraffin embedding. 4 μm paraffin sections on glass slides were used for H&E staining and images obtained on a standard light microscope.

Cell proliferation, neurogenesis and cell death analysis

$BACE1^{fl/fl}$ and $BACE1^{fl/fl}$;$R26CreER^{T2}$ mice received TAM injections at 6–9 months of age, were aged to 2 years, and then were treated with daily 50 μg/g BrdU i.p. injection for consecutive 7 days. Half of mice were collected 24hr and the rest 1 month after the last BrdU injection. Mice were perfused and processed for free floating brain section staining as described under *Tissue extraction and immunoblot analysis* and *Immunohistochemistry* sections. Every sixth section was used for measuring cell proliferation. GCL area was obtained by hand-tracing on 10X images in Image J. Volume was estimated by multiplying area with the distance spaced between sections. The number of BrdU+ cells was estimated by (number of BrdU+ cells counted) / (GCL volume). For neurogenesis experiments, every third section was co-labeled for BrdU and NeuN. A minimum of 10 BrdU positive cells was counted. Co-localization of BrdU and NeuN was confirmed by confocal microscopy. For regional analyses, the GCL was subdivided into *crest* defined as the first ¼ in length of suprapyramidal and infrapyramidal blades at the junction, and the rest of the *suprapyramidal* and *intrapyramidal* blades minus crest. The same BrdU+ cells counted in previous cell proliferation and neurogenesis experiments were divided into these three regions based on their location. For an estimate of total number of BrdU+ cells in sub-regions of the dentate gyrus (DG), the previously counted number of BrdU+ cells in each sub-region was multiplied by 6 (i.e., the number of intervening sections) in S12F. For cell death detection, sections were permeabilized with Triton X-100 for an hour followed by one hour incubation of reaction mix from *In Situ* Cell Death Detection Kit, TMR Red (Sigma, 12156792910 Roche) at 37°C.

Statistics

Statistics were calculated using Prism 5 (GraphPad Software). Repeated two-way ANOVA was used in hidden platform training in the Morris water maze test (Fig. 2A, 2C). One-way ANOVA was applied in the Morris water maze probe trials (Fig. 2B, 2D), spike-wave discharge/hour (Fig. 3C) and sciatic nerve MBP (Fig. 4B). Linear regression analyses were used in g-ratio analysis (Fig. 4E) and correlation between CHL1 and infrapyramidal bundle lengths (Fig. 5F and 5G). Chi-squared analysis was applied for BACE1$^{fl/fl}$;CamKIIα-iCre postnatal lethality (Fig. S5A). Unpaired two-way Student's t test was used in the rest of the data analysis. Numbers of replicates and p values are stated in each figure legend. All data are plotted as mean ± standard error of the mean (SEM). Significance was concluded when the p value was less than 0.05, indicated by * $p < 0.05$, ** $p<0.01$, ***$p<0.001$. N.S., not significant denotes $p>0.05$.

Supplementary Material

Refer to Web version on PubMed Central for supplementary material.

Acknowledgements

We thank members of the Vassar lab for helpful discussions, especially Trongha Phan and Katherine R. Sadleir. We thank Stefan Lichtenthalerfor generously sharing the Sez6 antibody. Behavioral analysis was supported in part by the Northwestern University Behavioral Phenotyping Core. Automated metabolic phenotyping was provided by Northwestern University Comprehensive Metabolic Core. BACE1$^{fl/fl}$ mice were generated with the assistance of Northwestern University Transgenic and Targeted Mutagenesis Laboratory. Necropsy services were supported by Lin Li and the Northwestern University Mouse Histology and Phenotyping Laboratory. Imaging work was performed at the Northwestern University Center for Advanced Microscopy.

Funding: This work was supported by NIH R01 AG022560, BrightFocus Foundation, and the Baila Foundation (to R.V.) and NIH K26 OD010945 and K02-NS046468 (to W.G.T.).

References

1. Tanzi RE, The genetics of Alzheimer disease. Cold Spring Harb Perspect Med 2, (2012).
2. Selkoe DJ, Hardy J, The amyloid hypothesis of Alzheimer's disease at 25 years. EMBO Mol Med 8, 595–608 (2016). [PubMed: 27025652]
3. Tanzi RE, Gusella JF, Watkins PC, Bruns GA, St George-Hyslop P, Van Keuren ML, Patterson D, Pagan S, Kurnit DM, Neve RL, Amyloid beta protein gene: cDNA, mRNA distribution, and genetic linkage near the Alzheimer locus. Science 235, 880–884 (1987). [PubMed: 2949367]
4. Haass C, Kaether C, Thinakaran G, Sisodia S, Trafficking and proteolytic processing of APP. Cold Spring Harb Perspect Med 2, a006270 (2012). [PubMed: 22553493]
5. Vassar R, Bennett BD, Babu-Khan S, Kahn S, Mendiaz EA, Denis P, Teplow DB, Ross S, Amarante P, Loeloff R, Luo Y, Fisher S, Fuller J, Edenson S, Lile J, Jarosinski MA, Biere AL, Curran E, Burgess T, Louis JC, Collins F, Treanor J, Rogers G, Citron M, Beta-secretase cleavage of Alzheimer's amyloid precursor protein by the transmembrane aspartic protease BACE. Science 286, 735–741 (1999). [PubMed: 10531052]
6. Yan R, Bienkowski MJ, Shuck ME, Miao H, Tory MC, Pauley AM, Brashier JR, Stratman NC, Mathews WR, Buhl AE, Carter DB, Tomasselli AG, Parodi LA, Heinrikson RL, Gurney ME, Membrane-anchored aspartyl protease with Alzheimer's disease beta-secretase activity. Nature 402, 533–537 (1999). [PubMed: 10591213]
7. Sinha S, Anderson JP, Barbour R, Basi GS, Caccavello R, Davis D, Doan M, Dovey HF, Frigon N, Hong J, Jacobson-Croak K, Jewett N, Keim P, Knops J, Lieberburg I, Power M, Tan H, Tatsuno G, Tung J, Schenk D, Seubert P, Suomensaari SM, Wang S, Walker D, Zhao J, McConlogue L, John V,

Purification and cloning of amyloid precursor protein beta-secretase from human brain. Nature 402, 537–540 (1999). [PubMed: 10591214]

8. Hussain I, Powell D, Howlett DR, Tew DG, Meek TD, Chapman C, Gloger IS, Murphy KE, Southan CD, Ryan DM, Smith TS, Simmons DL, Walsh FS, Dingwall C, Christie G, Identification of a novel aspartic protease (Asp 2) as beta-secretase. Mol Cell Neurosci 14, 419–427 (1999). [PubMed: 10656250]
9. Lin X, Koelsch G, Wu S, Downs D, Dashti A, Tang J, Human aspartic protease memapsin 2 cleaves the beta-secretase site of beta-amyloid precursor protein. Proceedings of the National Academy of Sciences of the United States of America 97, 1456–1460 (2000). [PubMed: 10677483]
10. Barao S, Moechars D, Lichtenthaler SF, De Strooper B, BACE1 Physiological Functions May Limit Its Use as Therapeutic Target for Alzheimer's Disease. Trends Neurosci 39, 158–169 (2016). [PubMed: 26833257]
11. Yan R, Vassar R, Targeting the beta secretase BACE1 for Alzheimer's disease therapy. The Lancet. Neurology 13, 319–329 (2014). [PubMed: 24556009]
12. Yan R, Physiological Functions of the beta-Site Amyloid Precursor Protein Cleaving Enzyme 1 and 2. Front Mol Neurosci 10, 97 (2017). [PubMed: 28469554]
13. Luo Y, Bolon B, Kahn S, Bennett BD, Babu-Khan S, Denis P, Fan W, Kha H, Zhang J, Gong Y, Martin L, Louis JC, Yan Q, Richards WG, Citron M, Vassar R, Mice deficient in BACE1, the Alzheimer's beta-secretase, have normal phenotype and abolished beta-amyloid generation. Nature neuroscience 4, 231–232 (2001). [PubMed: 11224535]
14. Cai H, Wang Y, McCarthy D, Wen H, Borchelt DR, Price DL, Wong PC, BACE1 is the major beta-secretase for generation of Abeta peptides by neurons. Nature neuroscience 4, 233–234 (2001). [PubMed: 11224536]
15. Roberds SL, Anderson J, Basi G, Bienkowski MJ, Branstetter DG, Chen KS, Freedman SB, Frigon NL, Games D, Hu K, Johnson-Wood K, Kappenman KE, Kawabe TT, Kola I, Kuehn R, Lee M, Liu W, Motter R, Nichols NF, Power M, Robertson DW, Schenk D, Schoor M, Shopp GM, Shuck ME, Sinha S, Svensson KA, Tatsuno G, Tintrup H, Wijsman J, Wright S, McConlogue L, BACE knockout mice are healthy despite lacking the primary beta-secretase activity in brain: implications for Alzheimer's disease therapeutics. Human molecular genetics 10, 1317–1324 (2001). [PubMed: 11406613]
16. Dominguez D, Tournoy J, Hartmann D, Huth T, Cryns K, Deforce S, Serneels L, Camacho IE, Marjaux E, Craessaerts K, Roebroek AJ, Schwake M, D'Hooge R, Bach P, Kalinke U, Moechars D, Alzheimer C, Reiss K, Saftig P, De Strooper B, Phenotypic and biochemical analyses of BACE1- and BACE2-deficient mice. The Journal of biological chemistry 280, 30797–30806 (2005). [PubMed: 15987683]
17. Willem M, Garratt AN, Novak B, Citron M, Kaufmann S, Rittger A, DeStrooper B, Saftig P, Birchmeier C, Haass C, Control of peripheral nerve myelination by the beta-secretase BACE1. Science 314, 664–666 (2006). [PubMed: 16990514]
18. Hu X, Hicks CW, He W, Wong P, Macklin WB, Trapp BD, Yan R, Bace1 modulates myelination in the central and peripheral nervous system. Nature neuroscience 9, 1520–1525 (2006). [PubMed: 17099708]
19. Hu X, Zhou X, He W, Yang J, Xiong W, Wong P, Wilson CG, Yan R, BACE1 deficiency causes altered neuronal activity and neurodegeneration. The Journal of neuroscience : the official journal of the Society for Neuroscience 30, 8819–8829 (2010). [PubMed: 20592204]
20. Hitt BD, Jaramillo TC, Chetkovich DM, Vassar R, BACE1−/− mice exhibit seizure activity that does not correlate with sodium channel level or axonal localization. Molecular neurodegeneration 5, 31 (2010). [PubMed: 20731874]
21. Laird FM, Cai H, Savonenko AV, Farah MH, He K, Melnikova T, Wen H, Chiang HC, Xu G, Koliatsos VE, Borchelt DR, Price DL, Lee HK, Wong PC, BACE1, a major determinant of selective vulnerability of the brain to amyloid-beta amyloidogenesis, is essential for cognitive, emotional, and synaptic functions. The Journal of neuroscience : the official journal of the Society for Neuroscience 25, 11693–11709 (2005). [PubMed: 16354928]
22. Ohno M, Chang L, Tseng W, Oakley H, Citron M, Klein WL, Vassar R, Disterhoft JF, Temporal memory deficits in Alzheimer's mouse models: rescue by genetic deletion of BACE1. The European journal of neuroscience 23, 251–260 (2006). [PubMed: 16420434]

23. Rajapaksha TW, Eimer WA, Bozza TC, Vassar R, The Alzheimer's beta-secretase enzyme BACE1 is required for accurate axon guidance of olfactory sensory neurons and normal glomerulus formation in the olfactory bulb. Molecular neurodegeneration 6, 88 (2011). [PubMed: 22204380]
24. Hitt B, Riordan SM, Kukreja L, Eimer WA, Rajapaksha TW, Vassar R, beta-Site amyloid precursor protein (APP)-cleaving enzyme 1 (BACE1)-deficient mice exhibit a close homolog of L1 (CHL1) loss-of-function phenotype involving axon guidance defects. The Journal of biological chemistry 287, 38408–38425 (2012). [PubMed: 22988240]
25. Cao L, Rickenbacher GT, Rodriguez S, Moulia TW, Albers MW, The precision of axon targeting of mouse olfactory sensory neurons requires the BACE1 protease. Scientific reports 2, 231 (2012). [PubMed: 22355745]
26. Barao S, Gartner A, Leyva-Diaz E, Demyanenko G, Munck S, Vanhoutvin T, Zhou L, Schachner M, Lopez-Bendito G, Maness PF, De Strooper B, Antagonistic Effects of BACE1 and APH1B-gamma-Secretase Control Axonal Guidance by Regulating Growth Cone Collapse. Cell reports 12, 1367–1376 (2015). [PubMed: 26299962]
27. Vassar R, Kovacs DM, Yan R, Wong PC, The beta-secretase enzyme BACE in health and Alzheimer's disease: regulation, cell biology, function, and therapeutic potential. The Journal of neuroscience : the official journal of the Society for Neuroscience 29, 12787–12794 (2009). [PubMed: 19828790]
28. Yan R, Stepping closer to treating Alzheimer's disease patients with BACE1 inhibitor drugs. Transl Neurodegener 5, 13 (2016). [PubMed: 27418961]
29. Casanova E, Fehsenfeld S, Mantamadiotis T, Lemberger T, Greiner E, Stewart AF, Schutz G, A CamKIIalpha iCre BAC allows brain-specific gene inactivation. Genesis 31, 37–42 (2001). [PubMed: 11668676]
30. Ventura A, Kirsch DG, McLaughlin ME, Tuveson DA, Grimm J, Lintault L, Newman J, Reczek EE, Weissleder R, Jacks T, Restoration of p53 function leads to tumour regression in vivo. Nature 445, 661–665 (2007). [PubMed: 17251932]
31. Zhou L, Barao S, Laga M, Bockstael K, Borgers M, Gijsen H, Annaert W, Moechars D, Mercken M, Gevaert K, De Strooper B, The neural cell adhesion molecules L1 and CHL1 are cleaved by BACE1 protease in vivo. The Journal of biological chemistry 287, 25927–25940 (2012). [PubMed: 22692213]
32. Kuhn PH, Koroniak K, Hogl S, Colombo A, Zeitschel U, Willem M, Volbracht C, Schepers U, Imhof A, Hoffmeister A, Haass C, Rossner S, Brase S, Lichtenthaler SF, Secretome protein enrichment identifies physiological BACE1 protease substrates in neurons. The EMBO journal 31, 3157–3168 (2012). [PubMed: 22728825]
33. Meakin PJ, Harper AJ, Hamilton DL, Gallagher J, McNeilly AD, Burgess LA, Vaanholt LM, Bannon KA, Latcham J, Hussain I, Speakman JR, Howlett DR, Ashford ML, Reduction in BACE1 decreases body weight, protects against diet-induced obesity and enhances insulin sensitivity in mice. Biochem J 441, 285–296 (2012). [PubMed: 21880018]
34. Savonenko AV, Melnikova T, Laird FM, Stewart KA, Price DL, Wong PC, Alteration of BACE1-dependent NRG1/ErbB4 signaling and schizophrenia-like phenotypes in BACE1-null mice. Proceedings of the National Academy of Sciences of the United States of America 105, 5585–5590 (2008). [PubMed: 18385378]
35. Montag-Sallaz M, Schachner M, Montag D, Misguided axonal projections, neural cell adhesion molecule 180 mRNA upregulation, and altered behavior in mice deficient for the close homolog of L1. Mol Cell Biol 22, 7967–7981 (2002). [PubMed: 12391163]
36. Heyden A, Angenstein F, Sallaz M, Seidenbecher C, Montag D, Abnormal axonal guidance and brain anatomy in mouse mutants for the cell recognition molecules close homolog of L1 and NgCAM-related cell adhesion molecule. Neuroscience 155, 221–233 (2008). [PubMed: 18588951]
37. Huang X, Zhu LL, Zhao T, Wu LY, Wu KW, Schachner M, Xiao ZC, Fan M, CHL1 negatively regulates the proliferation and neuronal differentiation of neural progenitor cells through activation of the ERK1/2 MAPK pathway. Mol Cell Neurosci 46, 296–307 (2011). [PubMed: 20933598]
38. Jakovcevski I, Siering J, Hargus G, Karl N, Hoelters L, Djogo N, Yin S, Zecevic N, Schachner M, Irintchev A, Close homologue of adhesion molecule L1 promotes survival of Purkinje and granule cells and granule cell migration during murine cerebellar development. J Comp Neurol 513, 496–510 (2009). [PubMed: 19226508]

39. Tian N, Leshchyns'ka I, Welch JH, Diakowski W, Yang H, Schachner M, Sytnyk V, Lipid raft-dependent endocytosis of close homolog of adhesion molecule L1 (CHL1) promotes neuritogenesis. The Journal of biological chemistry 287, 44447–44463 (2012). [PubMed: 23144456]
40. Katic J, Loers G, Kleene R, Karl N, Schmidt C, Buck F, Zmijewski JW, Jakovcevski I, Preissner KT, Schachner M, Interaction of the cell adhesion molecule CHL1 with vitronectin, integrins, and the plasminogen activator inhibitor-2 promotes CHL1-induced neurite outgrowth and neuronal migration. The Journal of neuroscience : the official journal of the Society for Neuroscience 34, 14606–14623 (2014). [PubMed: 25355214]
41. Demyanenko GP, Halberstadt AI, Rao RS, Maness PF, CHL1 cooperates with PAK1–3 to regulate morphological differentiation of embryonic cortical neurons. Neuroscience 165, 107–115 (2010). [PubMed: 19819308]
42. Kleene R, Chaudhary H, Karl N, Katic J, Kotarska A, Guitart K, Loers G, Schachner M, Interaction between CHL1 and serotonin receptor 2c regulates signal transduction and behavior in mice. J Cell Sci 128, 4642–4652 (2015). [PubMed: 26527397]
43. Demyanenko GP, Schachner M, Anton E, Schmid R, Feng G, Sanes J, Maness PF, Close homolog of L1 modulates area-specific neuronal positioning and dendrite orientation in the cerebral cortex. Neuron 44, 423–437 (2004). [PubMed: 15504324]
44. Ye H, Tan YL, Ponniah S, Takeda Y, Wang SQ, Schachner M, Watanabe K, Pallen CJ, Xiao ZC, Neural recognition molecules CHL1 and NB-3 regulate apical dendrite orientation in the neocortex via PTP alpha. The EMBO journal 27, 188–200 (2008). [PubMed: 18046458]
45. Hu X, He W, Luo X, Tsubota KE, Yan R, BACE1 regulates hippocampal astrogenesis via the Jagged1-Notch pathway. Cell reports 4, 40–49 (2013). [PubMed: 23831026]
46. van Praag H, Shubert T, Zhao C, Gage FH, Exercise enhances learning and hippocampal neurogenesis in aged mice. The Journal of neuroscience : the official journal of the Society for Neuroscience 25, 8680–8685 (2005). [PubMed: 16177036]
47. Jinno S, Decline in adult neurogenesis during aging follows a topographic pattern in the mouse hippocampus. J Comp Neurol 519, 451–466 (2011). [PubMed: 21192078]
48. Kandalepas PC, Sadleir KR, Eimer WA, Zhao J, Nicholson DA, Vassar R, The Alzheimer's beta-secretase BACE1 localizes to normal presynaptic terminals and to dystrophic presynaptic terminals surrounding amyloid plaques. Acta neuropathologica 126, 329–352 (2013). [PubMed: 23820808]
49. Zhao J, Fu Y, Yasvoina M, Shao P, Hitt B, O'Connor T, Logan S, Maus E, Citron M, Berry R, Binder L, Vassar R, Beta-site amyloid precursor protein cleaving enzyme 1 levels become elevated in neurons around amyloid plaques: implications for Alzheimer's disease pathogenesis. The Journal of neuroscience : the official journal of the Society for Neuroscience 27, 3639–3649 (2007). [PubMed: 17409228]
50. Faulkner RL, Jang MH, Liu XB, Duan X, Sailor KA, Kim JY, Ge S, Jones EG, Ming GL, Song H, Cheng HJ, Development of hippocampal mossy fiber synaptic outputs by new neurons in the adult brain. Proceedings of the National Academy of Sciences of the United States of America 105, 14157–14162 (2008). [PubMed: 18780780]
51. Toni N, Laplagne DA, Zhao C, Lombardi G, Ribak CE, Gage FH, Schinder AF, Neurons born in the adult dentate gyrus form functional synapses with target cells. Nature neuroscience 11, 901–907 (2008). [PubMed: 18622400]
52. Goncalves JT, Schafer ST, Gage FH, Adult Neurogenesis in the Hippocampus: From Stem Cells to Behavior. Cell 167, 897–914 (2016). [PubMed: 27814520]
53. Crusio WE, Schwegler H, Learning spatial orientation tasks in the radial-maze and structural variation in the hippocampus in inbred mice. Behav Brain Funct 1, 3 (2005). [PubMed: 15916698]
54. Wang H, Song L, Laird F, Wong PC, Lee HK, BACE1 knock-outs display deficits in activity-dependent potentiation of synaptic transmission at mossy fiber to CA3 synapses in the hippocampus. The Journal of neuroscience : the official journal of the Society for Neuroscience 28, 8677–8681 (2008). [PubMed: 18753368]
55. Wang H, Song L, Lee A, Laird F, Wong PC, Lee HK, Mossy fiber long-term potentiation deficits in BACE1 knock-outs can be rescued by activation of alpha7 nicotinic acetylcholine receptors.

The Journal of neuroscience : the official journal of the Society for Neuroscience 30, 13808–13813 (2010). [PubMed: 20943921]

56. Imayoshi I, Sakamoto M, Ohtsuka T, Takao K, Miyakawa T, Yamaguchi M, Mori K, Ikeda T, Itohara S, Kageyama R, Roles of continuous neurogenesis in the structural and functional integrity of the adult forebrain. Nature neuroscience 11, 1153–1161 (2008). [PubMed: 18758458]
57. Oakley H, Cole SL, Logan S, Maus E, Shao P, Craft J, Guillozet-Bongaarts A, Ohno M, Disterhoft J, Van Eldik L, Berry R, Vassar R, Intraneuronal beta-amyloid aggregates, neurodegeneration, and neuron loss in transgenic mice with five familial Alzheimer's disease mutations: potential factors in amyloid plaque formation. The Journal of neuroscience : the official journal of the Society for Neuroscience 26, 10129–10140 (2006). [PubMed: 17021169]
58. Hu X, Das B, Hou H, He W, Yan R, BACE1 deletion in the adult mouse reverses preformed amyloid deposition and improves cognitive functions. The Journal of experimental medicine, (2018).
59. Kennedy ME, Stamford AW, Chen X, Cox K, Cumming JN, Dockendorf MF, Egan M, Ereshefsky L, Hodgson RA, Hyde LA, Jhee S, Kleijn HJ, Kuvelkar R, Li W, Mattson BA, Mei H, Palcza J, Scott JD, Tanen M, Troyer MD, Tseng JL, Stone JA, Parker EM, Forman MS, The BACE1 inhibitor verubecestat (MK-8931) reduces CNS beta-amyloid in animal models and in Alzheimer's disease patients. Sci Transl Med 8, 363ra150 (2016).
60. Egan MF, Kost J, Tariot PN, Aisen PS, Cummings JL, Vellas B, Sur C, Mukai Y, Voss T, Furtek C, Mahoney E, Harper Mozley L, Vandenberghe R, Mo Y, Michelson D, Randomized Trial of Verubecestat for Mild-to-Moderate Alzheimer's Disease. N Engl J Med 378, 1691–1703 (2018). [PubMed: 29719179]
61. May PC, Willis BA, Lowe SL, Dean RA, Monk SA, Cocke PJ, Audia JE, Boggs LN, Borders AR, Brier RA, Calligaro DO, Day TA, Ereshefsky L, Erickson JA, Gevorkyan H, Gonzales CR, James DE, Jhee SS, Komjathy SF, Li L, Lindstrom TD, Mathes BM, Martenyi F, Sheehan SM, Stout SL, Timm DE, Vaught GM, Watson BM, Winneroski LL, Yang Z, Mergott DJ, The potent BACE1 inhibitor LY2886721 elicits robust central Abeta pharmacodynamic responses in mice, dogs, and humans. The Journal of neuroscience : the official journal of the Society for Neuroscience 35, 1199–1210 (2015). [PubMed: 25609634]
62. Sakamoto K, Matsuki S, Matsuguma K, Yoshihara T, Uchida N, Azuma F, Russell M, Hughes G, Haeberlein SB, Alexander RC, Eketjall S, Kugler AR, BACE1 Inhibitor Lanabecestat (AZD3293) in a Phase 1 Study of Healthy Japanese Subjects: Pharmacokinetics and Effects on Plasma and Cerebrospinal Fluid Abeta Peptides. J Clin Pharmacol, (2017).
63. Spalding KL, Bergmann O, Alkass K, Bernard S, Salehpour M, Huttner HB, Bostrom E, Westerlund I, Vial C, Buchholz BA, Possnert G, Mash DC, Druid H, Frisen J, Dynamics of hippocampal neurogenesis in adult humans. Cell 153, 1219–1227 (2013). [PubMed: 23746839]
64. Nomura T, Oyamada Y, Fernandes HB, Remmers CL, Xu J, Meltzer HY, Contractor A, Subchronic phencyclidine treatment in adult mice increases GABAergic transmission and LTP threshold in the hippocampus. Neuropharmacology 100, 90–97 (2016). [PubMed: 25937215]

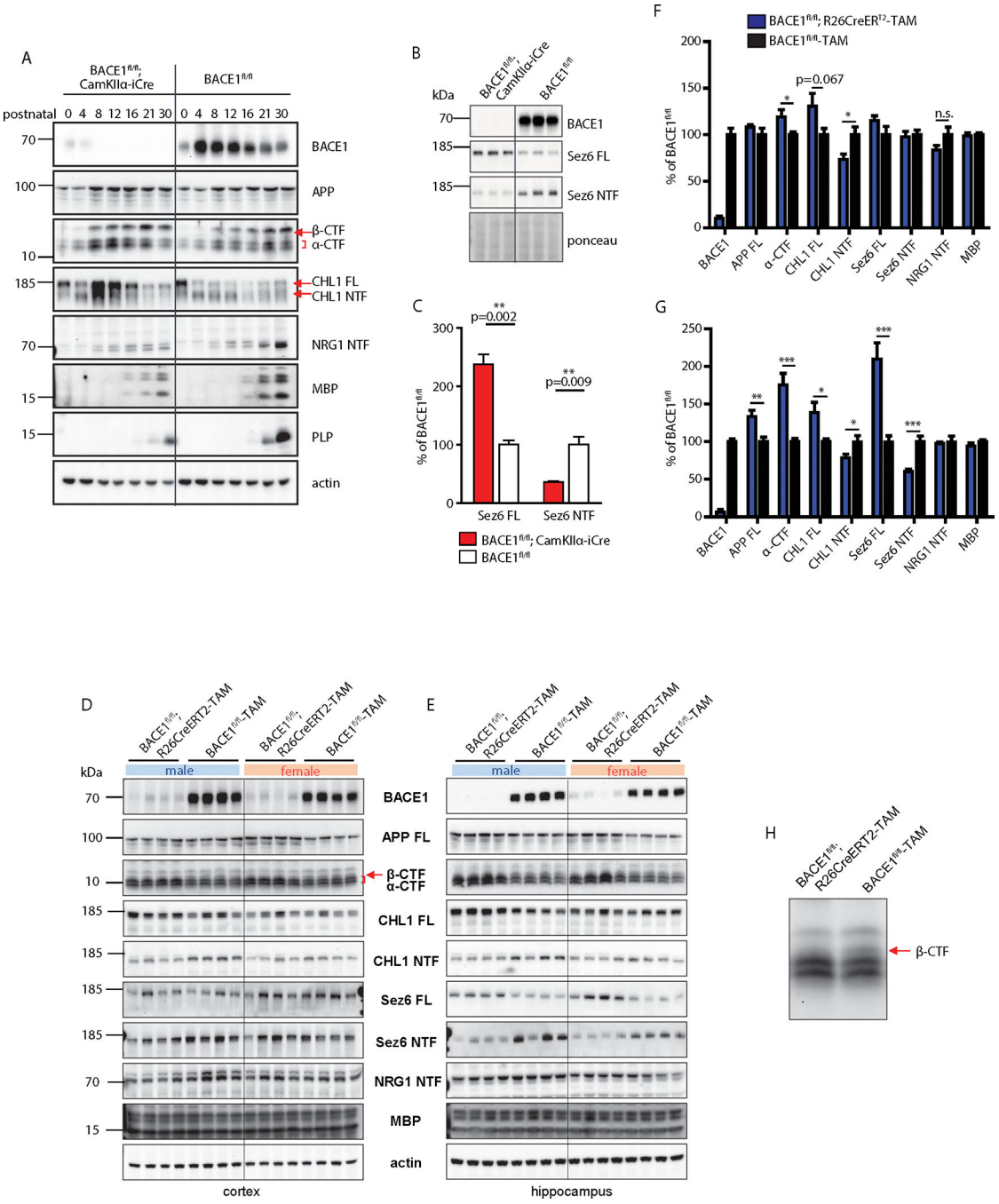

Fig. 1. Conditional BACE1 knockout mice exhibit robust reduction of BACE1 and cleavage of BACE1 substrates.

(A) Immunoblots of total cortical homogenates from postnatal BACE1$^{fl/fl}$;CamKIIα-iCre and BACE1$^{fl/fl}$ mice were probed with antibodies against BACE1 and the indicated full-length BACE1 substrates, BACE1-cleaved substrate fragments and myelin-associated proteins. **(B)** Immunoblots of cortical homogenates of 3 month-old BACE1$^{fl/fl}$;CamKIIα-iCre mice and BACE1$^{fl/fl}$ mice were probed with antibodies against BACE1 and the BACE1 substrate Sez6 in membrane (Sez6 full length, FL) and soluble (Sez6 amino-

terminal fragment, NTF) fractions. **(C)** Immunosignals shown in (B) were normalized to ponceau staining and represented as percentage of immunosignal in $BACE1^{fl/fl}$ mice. **(D, E)** Immunoblots of cortical (D) and hippocampal (E) soluble or membrane homogenates from $BACE1^{fl/fl}$ and $BACE1^{fl/fl}$;$R26CreER^{T2}$ mice that were treated with tamoxifen (TAM) at 3 months and analyzed at 1 year of age. Panels represent immunoblots of membrane (BACE1, APP FL, α/β-carboxy-terminal fragment, CTF, CHL1 FL, Sez6 FL, myelin basic protein, MBP) and soluble (CHL1 NTF, Sez6 NTF, NRG1 NTF) fractions of cortical or hippocampal homogenates. **(F, G)** Quantification of cortical (F) and hippocampal (G) immunoblot signals for BACE1, BACE1 substrates, and MBP in (D) and (E), respectively. Protein concentrations for tamoxifen-treated $BACE1^{fl/fl}$ and tamoxifen-treated $BACE1^{fl/fl}$;$R26CreER^{T2}$ mice were compared using unpaired two-way student's t tests. p values for cortex are: α-CTF, p=0.036; CHL1 NTF, p=0.024. p values for hippocampus are: APP FL, p= 0.0065; α-CTF: p= 0.00032; CHL1 FL, p= 0.015; CHL1 NTF, p= 0.039; Sez6 FL, p= 0.0003; Sez6 NTF, p= 0.0003. **(H)** Enlarged APP β-CTF immunoblot bands from lanes 12 and 13 of (D). FL, full-length; CTF: C-terminal fragment; NTF, N-terminal fragment.

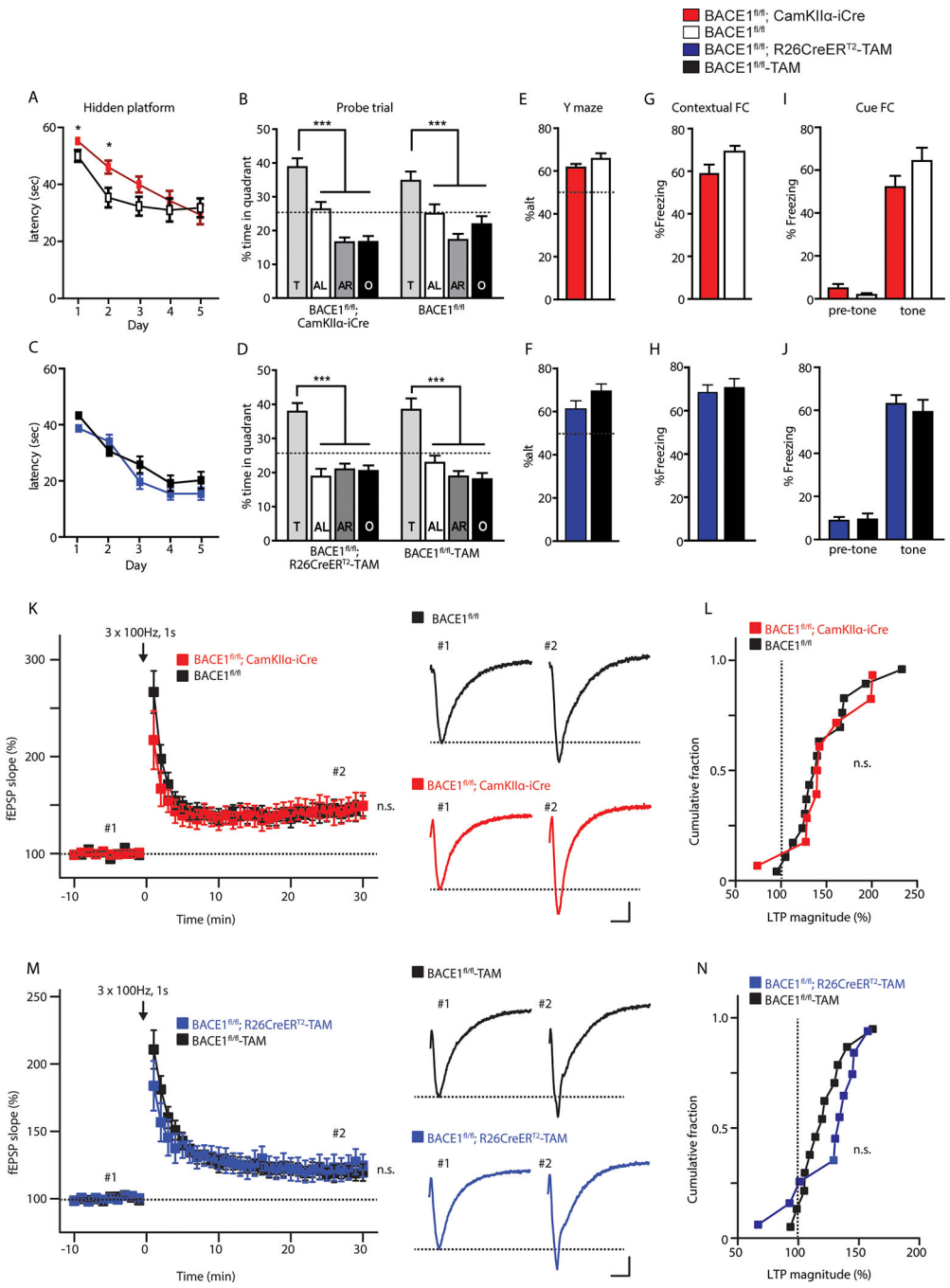

Fig. 2. Conditional BACE1 knockout mice lack memory deficits and LTP impairment.

BACE1$^{fl/fl}$;CamKIIα-iCre, tamoxifen-treated BACE1$^{fl/fl}$;R26CreER^{T2}, and respective control mice were assessed in the Morris water maze, Y-maze, fear conditioning, and longterm potentiation (LTP) tests. **(A-D)** Testing of conditional BACE1 knockout mice in the Morris Water Maze. **(A-B)** 9 month-old BACE1$^{fl/fl}$;CamKIIα-iCre (n=23) mice and BACE1$^{fl/fl}$ (n=18) mice were trained using **(A)** a hidden platform (Repeated two-way ANOVA, p=0.074, F=3.382), followed by **(B)** a probe trial test (One-way ANOVA, F_{CKO}=26.75, F_{CONT}=9.86). **(C-D)** BACE1$^{fl/fl}$;R26CreER^{T2}-TAM (n=17) mice and control

BACE1$^{fl/fl}$ -TAM (n=14) mice treated with tamoxifen (TAM) at 3 months were assessed in the Morris water maze at 9 months of age in **(C)** the hidden platform (Repeated 2-way ANOVA, p=0.089, F=3.096) followed by the **(D)** probe trial (One-way ANOVA, F_{CKO}=18.68, F_{CONT}=17.03). **(E, G, I)** BACE1$^{fl/fl}$;CamKIIα-iCre and BACE1$^{fl/fl}$ mice were tested in a Y-maze (E), and in tests measuring contextual fear conditioning (FC) and cued fear conditioning (G, I, respectively). N= (23, 18) for Y-Maze and (24, 16) for fear conditioning for BACE1$^{fl/fl}$;CamKIIα-iCre and BACE1$^{fl/fl}$ mice, respectively. **(F, H, J)** BACE1$^{fl/fl}$;R26CreER^{T2}-TAM and BACE1$^{fl/fl}$-TAM mice treated with tamoxifen were tested in a Y-maze (F), and in tests measuring contextual (H) and cued fear conditioning (J). N= (17, 13) for Y-maze and (17, 14) for fear conditioning for BACE1$^{fl/fl}$;R26CreER^{T2}-TAM and BACE1$^{fl/fl}$-TAM mice, respectively. **(K-N)** LTP in the CA1 region of the hippocampus. **(K)** Grouped data showing time-course of LTP for 1 year-old BACE1$^{fl/fl}$;CamKIIα-iCre mice (red, n=9 slices from 5 animals) and control BACE1$^{fl/fl}$ mice (white, n=15 slices from 5 animals). **(L)** Cumulative probability distribution of all LTP recordings in (K). **(M-N)** Grouped data showing time-course of LTP for 9 month-old BACE1$^{fl/fl}$;R26CreER^{T2}-TAM (blue, n=10 slices from 3 animals) and control BACE1$^{fl/fl}$-TAM mice (black, n=12 slices from 3 animals) that were injected with tamoxifen (TAM) at 3 months of age. **(N)** Cumulative probability distribution of all LTP recordings in (M). LTP was induced at time=0 with 3 trains of 100Hz, 1s tetanic stimulation (arrows in K and M). LTP statistics were analyzed by unpaired student's t test.

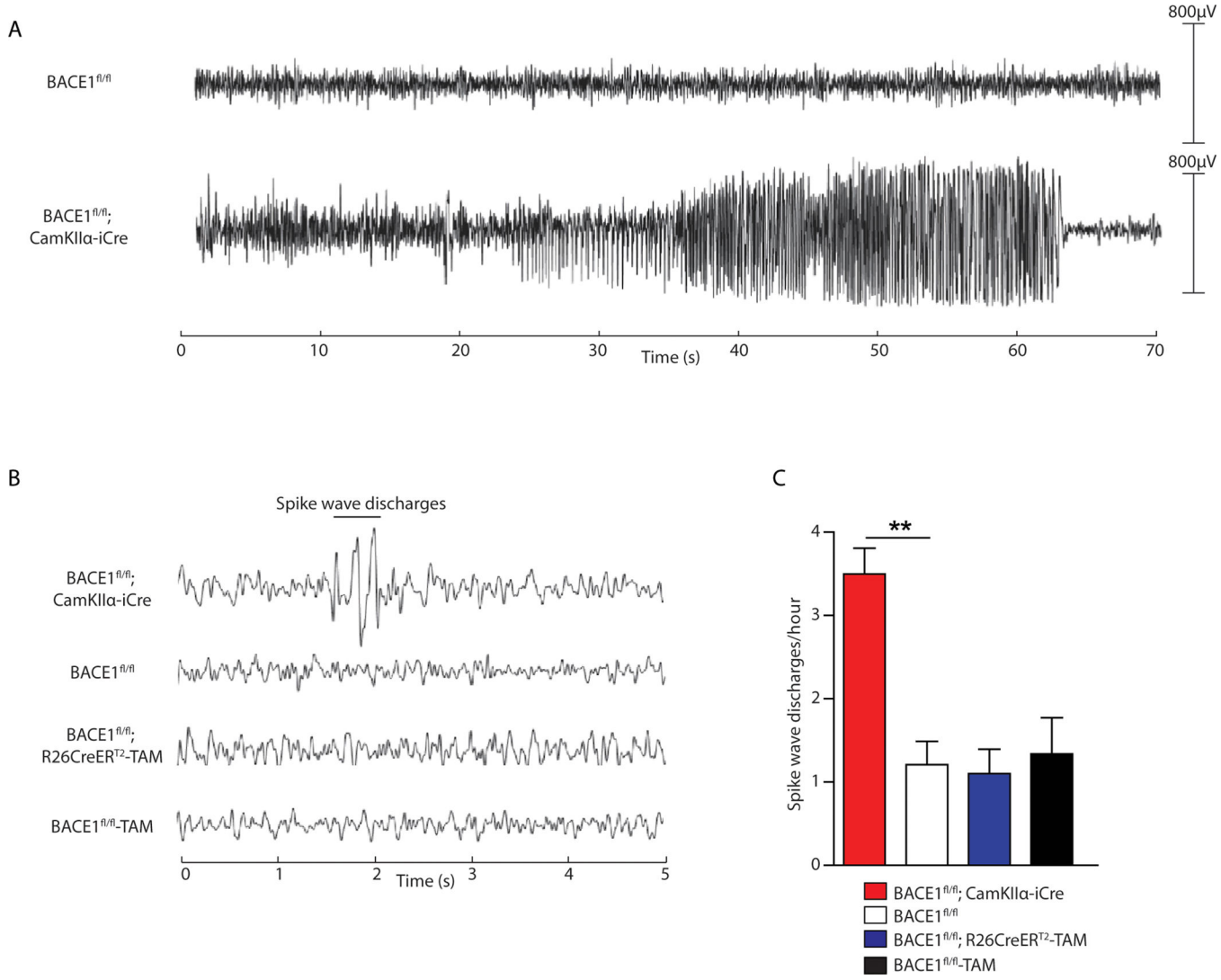

Fig. 3. Seizure activity was reduced or absent in BACE1 conditional knockout mice.

Seizure activity was measured in postnatal forebrain excitatory neuron BACE1 conditional knockout mice and in adult whole-body BACE1 conditional knockout mice. **(A)** Electrographic seizure with buildup of generalized fast activity in BACE1$^{fl/fl}$;CamKIIα-iCre mice at 1 year of age (lower panel) compared to age-matched BACE1$^{fl/fl}$ control mice (upper panel). **(B)** EEG in awake animals showed epileptiform abnormalities, including spike-wave discharges, in BACE1$^{fl/fl}$;CamKIIα-iCre mice (n=6) compared to normal EEG in BACE1$^{fl/fl}$ mice (n=4), BACE1$^{fl/fl}$-TAM mice treated with tamoxifen (n=5) and BACE1$^{fl/fl}$;R26CreER^{T2}-TAM mice treated with tamoxifen (n=6). **(C)** Comparison of the frequency of spike-wave discharges in mice with the four indicated genotypes: BACE1$^{fl/fl}$;CamKIIα-iCre, BACE1$^{fl/fl}$, BACE1$^{fl/fl}$;R26CreER^{T2}-TAM and BACE1$^{fl/fl}$-TAM. P values are 0.0003 by one-way ANOVA and 0.0011 by Tukey post-hoc test between BACE1$^{fl/fl}$;CamKIIα-iCre mice and BACE1$^{fl/fl}$ mice.

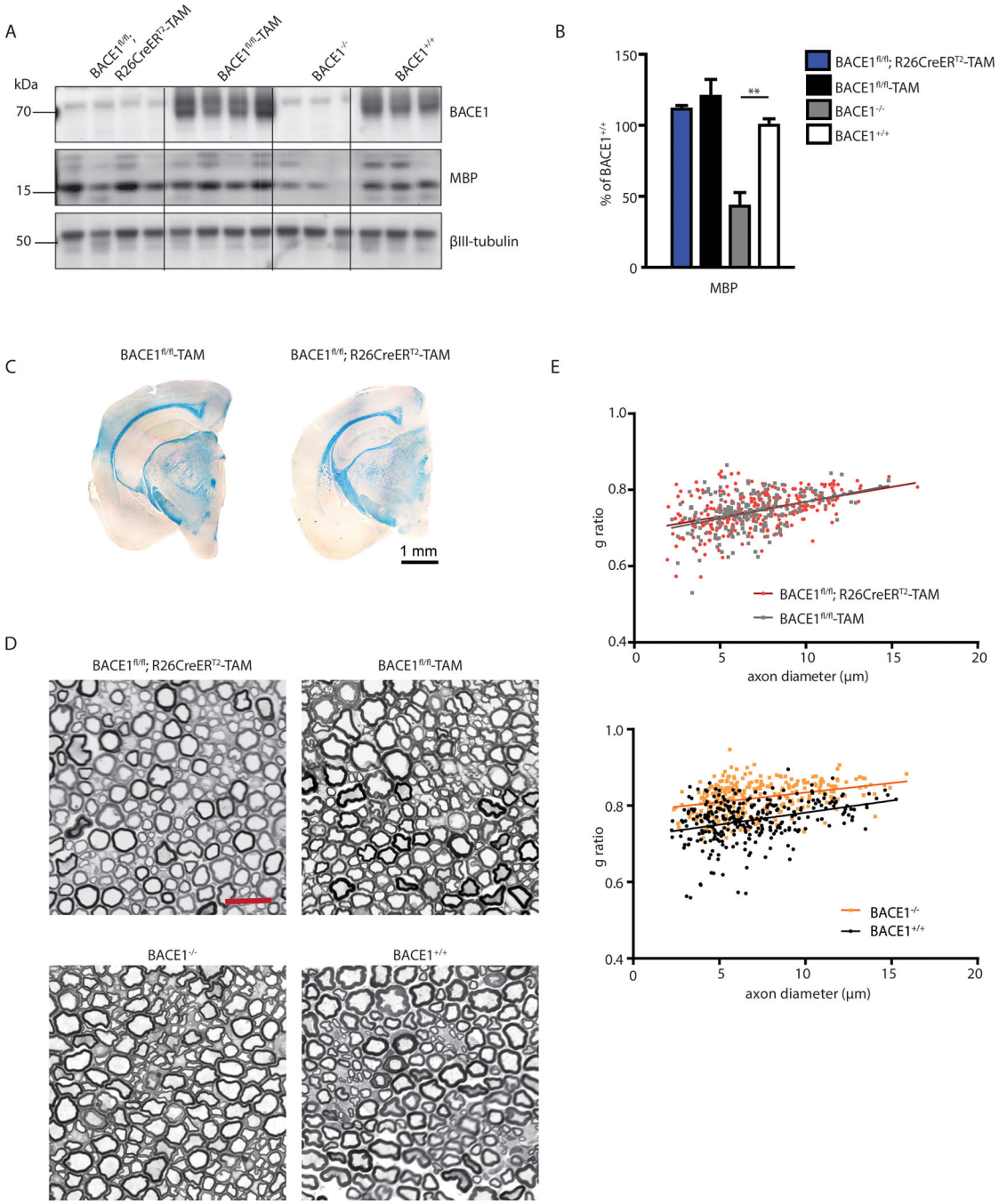

Fig. 4. Central and peripheral hypomyelination are absent in adult whole-body BACE1 conditional knockout mice.

(A) Immunoblot analysis of sciatic nerve homogenates showing BACE1 and myelin basic protein (MBP) in BACE1$^{fl/fl}$;R26CreER^{T2}-TAM, BACE1$^{fl/fl}$-TAM, BACE1$^{-/-}$, and BACE1$^{+/+}$ mice. **(B)** Quantification of MBP immunoblot signals from (A), normalized to βIII-tubulin immunosignal (One-way ANOVA on MBP, p=0.0004, F=15.9. P value of 0.006 from unpaired two-way student's t-test). **(C)** Luxol fast blue staining of myelinated fibers in BACE1$^{fl/fl}$;R26CreER^{T2}-TAM tamoxifen treated and control BACE1$^{fl/fl}$ mouse brains. **(D)**

Images of toluidine blue stained sciatic nerve thin sections showing myelination in $BACE1^{fl/fl}$;$R26CreER^{T2}$-TAM compared to $BACE1^{fl/fl}$-TAM tamoxifen treated mice and $BACE1^{-/-}$ compared to $BACE1^{+/+}$ mice. Scale bar = 20 μm. **(E)** Quantification of myelination via g-ratio between $BACE1^{fl/fl}$;$R26CreER^{T2}$-TAM tamoxifen treated (n=3) and $BACE1^{fl/fl}$-TAM tamoxifen treated (n=2) mice (upper panel; Linear regression analysis on slope: F=0.27, p=0.6; on intercepts: F=1.03, p=0.31), and $BACE1^{-/-}$ (n=3) mice and $BACE1^{+/+}$ (n=3) mice (lower panel). 100 axons per animal; Linear regression analysis on slope: F=0.98, p=0.32; on intercepts: F=233.6, p<0.0001.

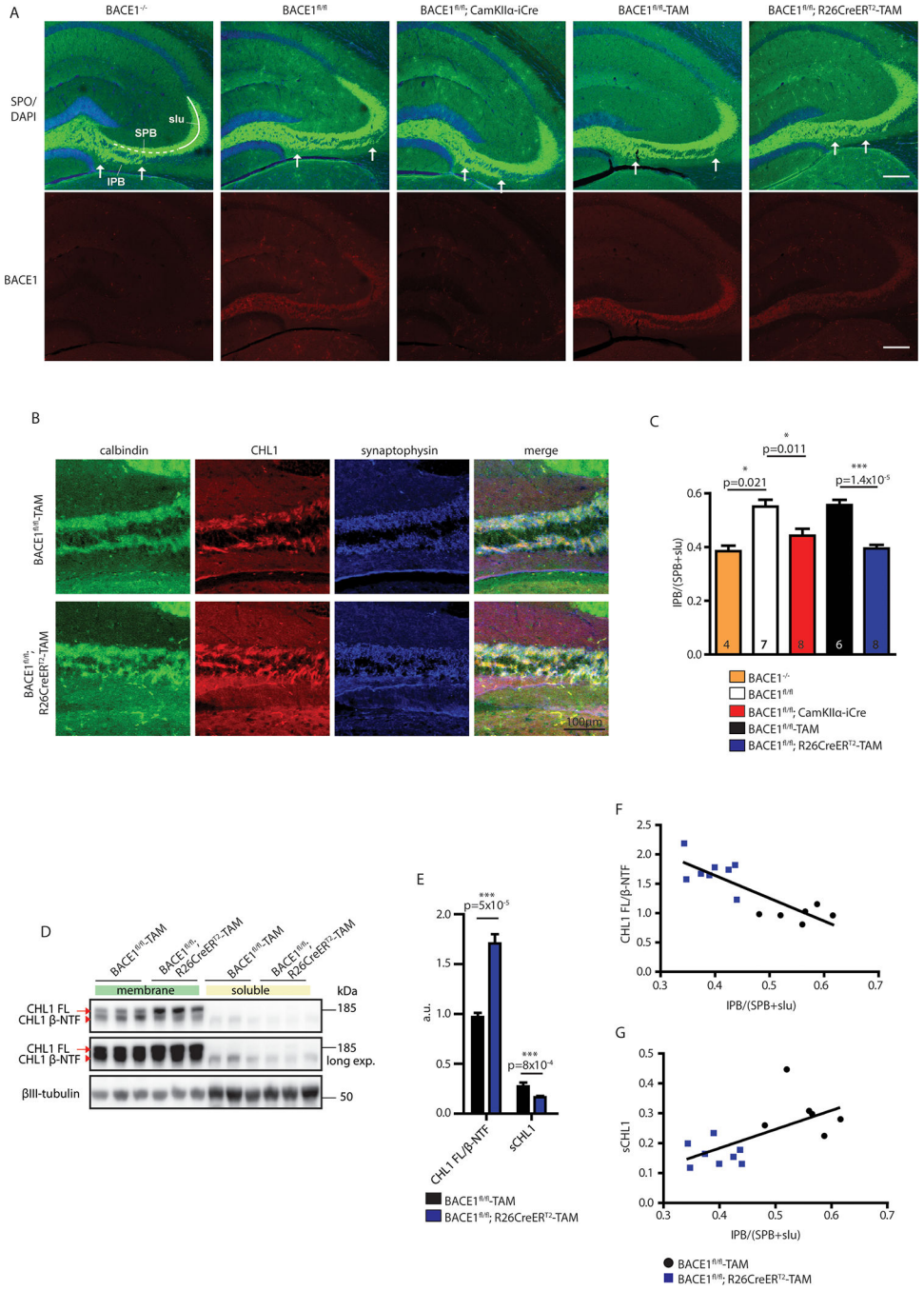

Fig. 5. Adult conditional BACE1 knockout mice show disorganization of the hippocampal mossy fiber pathway.

(A) Shown are coronal brain sections from mice with the indicated genotypes (BACE1$^{-/-}$, BACE1$^{fl/fl}$, BACE1$^{fl/fl}$;CamKIIα-iCre, BACE1$^{fl/fl}$-TAM, BACE1$^{fl/fl}$;R26CreER^{T2}-TAM) revealing the hippocampus co-labeled for the mossy fiber marker synaptoporin (SPO, green, upper panel) and BACE1 (red, lower panel). Arrows delineate the boundaries of the infrapyramidal bundle (IPB). BACE1$^{fl/fl}$-TAM and BACE1$^{fl/fl}$;R26CreER^{T2}-TAM mice

were treated with tamoxifen at 3 months of age and analyzed at 1 year of age. $BACE1^{-/-}$ and $BACE1^{fl/fl}$ mice at 9 month of age were used as positive and negative controls, respectively. SPB, suprapyramidal bundle; slu, stratum lucidum. Scale bar = 200μm. **(B)** Coronal brain sections from $BACE1^{fl/fl}$-TAM and $BACE1^{fl/fl}$;$R26CreER^{T2}$-TAM tamoxifen treated mice in (A) were co-immunostained with antibodies against CHL1 (red),the mossy fiber bouton and presynaptic terminal markers calbindin (green), and synaptophysin (blue). **(C)** Infrapyramidal bundle (IPB) lengths were normalized to the lengths of the suprapyramidal bundle (SPB) plus stratum lucidum (slu) and displayed as ratios, that is,IPB/(SPB+slu). The number of mice for each genotype is indicated in each bar of the graph. Error bars indicate standard error of the mean; p-values for indicated comparisons (lines) using unpaired Student's t test are shown above the bars. **(D)** Both soluble and membrane fractions were prepared from the hippocampi of representative $BACE1^{fl/fl}$-TAM and $BACE1^{fl/fl}$;$R26CreER^{T2}$-TAM tamoxifen treated mice and then were subjected to immunoblot analysis for full length (FL) CHL1 and CHL1 N-terminal fragment (β-NTF). Middle panel represents a longer exposure of the upper panel. βIII-tubulin was the loading control. **(E)** Ratio of CHL1 FL to CHL1 β-NTF intensities in membrane fractions (CHL1 FL/ β-NTF) and the intensity of the CHL1 β-NTF band in soluble fractions normalized to βIII-tubulin (sCHL1) displayed as arbitrary units (a.u.) for $BACE1^{fl/fl}$;$R26CreER^{T2}$-TAM and $BACE1^{fl/fl}$-TAM mice treated with tamoxifen, mean ± SEM. **(F)** Correlation of CHL1 FL/ β-NTF from (E) plotted against IPB/(SPB+slu) for $BACE1^{fl/fl}$;$R26CreER^{T2}$-TAM and $BACE1^{fl/fl}$-TAM tamoxifen treated mice (R^2=0.7014, p=0.0002). **(G)** Correlation of sCHL1 from (E) plotted against IPB/(SPB+slu) for $BACE1^{fl/fl}$;$R26CreER^{T2}$-TAM and $BACE1^{fl/fl}$-TAM tamoxifen treated mice (R^2=0.4117, p=0.01).